INFORMATION TO USERS

This manuscript has been reproduced from the microfilm master. UMI films the text directly from the original or copy submitted. Thus, some thesis and dissertation copies are in typewriter face, while others may be from any type of computer printer.

The quality of this reproduction is dependent upon the quality of the copy submitted. Broken or indistinct print, colored or poor quality illustrations and photographs, print bleedthrough, substandard margins, and improper alignment can adversely affect reproduction.

In the unlikely event that the author did not send UMI a complete manuscript and there are missing pages, these will be noted. Also, if unauthorized copyright material had to be removed, a note will indicate the deletion.

Oversize materials (e.g., maps, drawings, charts) are reproduced by sectioning the original, beginning at the upper left-hand corner and continuing from left to right in equal sections with small overlaps. Each original is also photographed in one exposure and is included in reduced form at the back of the book.

Photographs included in the original manuscript have been reproduced xerographically in this copy. Higher quality 6" x 9" black and white photographic prints are available for any photographs or illustrations appearing in this copy for an additional charge. Contact UMI directly to order.

UMI

MUSCLE COORDINATION OF THE HUMAN INDEX FINGER

A DISSERTATION

SUBMITTED TO THE DEPARTMENT OF MECHANICAL ENGINEERING

AND THE COMMITTEE ON GRADUATE STUDIES

OF STANFORD UNIVERSITY

IN PARTIAL FULFILLMENT OF THE REQUIREMENTS

FOR THE DEGREE OF

DOCTOR OF PHILOSOPHY

Francisco Javier Valero Cuevas

April 1997

UMI Number: 9802133

UMI Microform 9802133
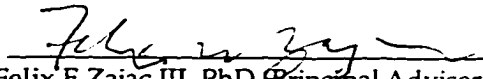Copyright 1997, by UMI Company. All rights reserved.

This microform edition is protected against unauthorized
copying under Title 17, United States Code.

UMI

300 North Zeeb Road
Ann Arbor, MI 48103

I certify that I have read this dissertation and that in my opinion it is fully adequate, in scope and quality, as a dissertation for the degree of Doctor of Philosophy.

Felix E Zajac III, PhD (Principal Adviser)

I certify that I have read this dissertation and that in my opinion it is fully adequate, in scope and quality, as a dissertation for the degree of Doctor of Philosophy.

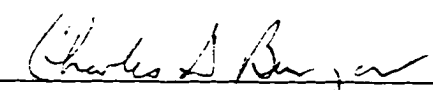Kai-Nan An, PhD (Bioengineering, Mayo Medical School)

I certify that I have read this dissertation and that in my opinion it is fully adequate, in scope and quality, as a dissertation for the degree of Doctor of Philosophy.

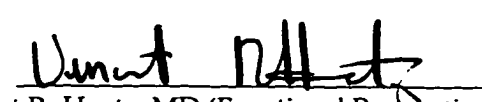Charles G. Burgar, MD (Functional Restoration)

I certify that I have read this dissertation and that in my opinion it is fully adequate, in scope and quality, as a dissertation for the degree of Doctor of Philosophy.

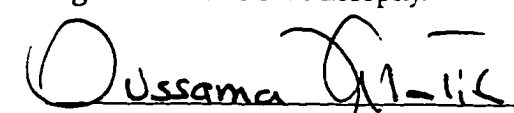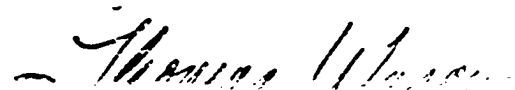Vincent R. Hentz, MD (Functional Restoration)

I certify that I have read this dissertation and that in my opinion it is fully adequate, in scope and quality, as a dissertation for the degree of Doctor of Philosophy.

Oussama Khatib, PhD (Computer Science)

Approved for the University Committee on Graduate Studies:

ABSTRACT

Surgical reconstruction of the hand often targets restoration of tip and key pinch, which involves the generation of force by the thumb and the index finger in a specific finger/thumb posture. We report muscle coordination patterns associated with production of maximal force by the index-finger at the distal phalanx in three orthogonal directions. A 3-dimensional, 7-muscle model of the finger reproduced the force and coordination observed with palmar and distal force generation. Analysis of the model showed that palmar force is most sensitive to flexor moment arms at the proximal interphalangeal joint, distal force to dorsal interosseous force production, and lateral force to extensor force production. However, interossei co-excitation observed in lateral force production could not be replicated. One explanation considered was that the model of the metacarpophalangeal joint should include a supination-pronation degree-of-freedom (DOF). However, the addition of a supination-pronation DOF severely compromises the inherent capability of the finger model to produce lateral force. It is concluded that supination-pronation is probably not an independent kinematic DOF at the MCP, and that co-excitation of the interossei may simply be an injury prevention strategy. Lastly, the implications of the multiarticular function of finger muscles are presented in the context of tendon transfers. Specifically, it is believed grasping force could be enhanced should the moment arm of flexor profundus at the proximal interphalangeal joint be increased after a Zancolli Lasso, which is a tendon transfer to correct post-paralysis finger deformity.

TABLE OF CONTENTS

LIST OF TABLES

LIST OF ILLUSTRATIONS

> *"[The universe] cannot be read until we have learnt the language and become familiar with the characters in which it is written. It is written in mathematical language, and the letters are triangles, circles and other geometrical figures, without which means it is humanly impossible to comprehend a single word."*
>
> *"Measure what is measurable, and make measurable what is not so."*
>
> Galileo Galilei (1564 - 1642)

INTRODUCTION

PREFACE

You have just accomplished an astonishing feat of dexterity. To flip to this page, you have effortlessly and precisely controlled at least 16 muscles and 10 joints in your thumb and index-finger. Many are not as fortunate as you. Injury or disease has deprived thousands of people of effective control over some or all of these muscles, thereby compromising their grasping ability. Finger and thumb function are the foundations of grasp. Understandably, clinicians and researchers have sought to understand, first, how finger musculature is coordinated to produce grasp, and, second, what can be done clinically and surgically to best restore adequate grasping function following injury or disease.

The sheer biomechanical complexity of the human hand, and our inability to easily record neural motor commands directly, have hindered our progress towards understanding finger function in grasping. When realized, this understanding holds the promise of rewarding us with techniques to restore grasp for generations to come. I hope this work contributes to our understanding of finger function, and brings us one step closer to its application to the functional restoration of grasp. I also hope this work is worthy of being considered part of the long tradition that uses mathematical concepts to bring the beauty of living systems into focus and perspective.

ACKNOWLEDGMENTS

A doctoral dissertation, like a Zen *koan*, draws much of its meaning from what is not included in it—the dead ends, the exhilarating moments of creativity and discovery, and the friends along the way. Throughout it all, the boundless love, good humor, hard work and unconditional support of my companion Erika made it an amazing, unforgettable experience.

I owe Dr. Felix Zajac a debt of gratitude for giving me the opportunity to learn to do Science under his outstanding tutelage. He has a gift for fostering intellectual creativity and independence while consistently upholding a superior standard of quality and fairness. He literally went "out on a (upper) limb" to support my interests, and I cannot thank him enough for that. Dr. Kai-Nan An was instrumental to the success of this work by enthusiastically encouraging me and steering my interests with his profound knowledge on the subject of Biomechanics—from 1,665 miles away. He provided me a complete set of moment arm data, invited me to his laboratory to implement the prototype of the force measurement technique, and advised me on EMG recording protocol. Much of this work could not have been accomplished if it were not for the remarkable array of skills Dr. Charles "Chuck" Burgar has for getting things done well. He also put up with my questions with endless patience, and shared with me his broad knowledge on other important subjects ranging from the habits of the op-amps to the quirks of the manta ray. Dr. Vincent R. Hentz added the crucial component of vision to this work by generously giving of his scarce time to introduce me to the delicate work of the Surgeon, and to guide me through the awesome beauty of the anatomy and function of the hand. He also showed me how loving one's work is the best way to do it well.

My fellow graduate students of the Neuromuscular Systems Laboratory gave me endless hours of intellectual, humorous and personal interaction that made these years seem too short. In particular, Art Kuo is a friend who, even after he finished here, has kept me on my toes with challenging ideas and good company. Pete Loan and Carlos Benitez are two great guys with whom

its was a pleasure to work. The quick mind and quicker wit of Chris Raasch made lunch a time to savor, figuratively. Lena Ting and Sydney Roberts are prove positive that life is a great adventure. I enjoyed living vicariously in the stage limelight through Kit Runge, and in the cycling world through Fran Sheehan.

Stanford, California.

OUTLINE

Chapter I: Biomechanical factors limiting index-finger force production.

The coordination of finger muscles is considered biomechanically redundant because several different muscle excitation patterns may produce the same finger force. This study applies an experimental-theoretical method to find the unique muscle excitation pattern that produces the maximal finger force of a biomechanical system with an arbitrary number of muscles and joints. In essence, a mathematical model of the system predicts unique muscle excitation patterns by combining the mechanical characteristics of well defined motor tasks and the mathematical uniqueness of control strategies that achieve the limits of performance. The method was applied to experimental measurements of finger forces and muscle activity. The model could reproduce most of the measurements. The model was also used to find the biomechanical factors that affect finger force magnitudes most.

Chapter II: Implications of metacarpo-phalangeal joint kinematics to the force production capabilities of a 3D index-finger model.

The model in Chapter I was not able to replicate some of the recorded muscle excitation patterns during the production of finger tip forces directed towards the sides of the finger. Because these finger forces are produced by muscles acting on the joint at the base of the finger, two alternative mechanical descriptions of this joint were explored in this study. It is concluded that these alternative descriptions result in problematic force magnitude predictions. This suggests that complementing the original model with muscle strategies that prevent joint damage, rather than modifying the description of the joint at the base of the finger, may reproduce the muscle excitation patterns recorded for lateral finger forces while predicting realistic force magnitudes.

4

Chapter III: Clinical implications

The third and last study explores the factors and principles found in this work that may be clinically or surgically applicable to the functional restoration of grasp. I discuss the design of tendon transfers, the role of the extensor mechanism in distributing tendon forces and the indirect estimation of the fiber length of a muscle relative to its optimal length.

Appendix A: Fine wire recordings from the muscle of the index-finger

It is difficult to record neural motor commands directly. A practical alternative is to use the bio-electrical activity present in a muscle during force production as an indirect estimate of the neural command to that muscle. The complex anatomy of index-finger musculature poses special problems to the accurate placement of the temporary electrodes used to record this activity. This section presents novel approaches to some of these muscles and electrode guidance techniques developed by Dr. Charles G. Burgar, Dr. Vincent R. Hentz and myself.

Appendix B: Additional data

The experimental and theoretical scope of this work covered the production of index-finger forces in five different directions in three standardized finger postures. However, only data for the more functionally or clinically relevant finger forces and postures are presented in the above studies. This section contains additional experimental recordings and model predictions.

Appendix C: Sample calculation of feasible force set

This section presents the calculation of the predicted maximal forces in the plane of finger flexion.

CHAPTER I: MUSCULOSKELETAL FACTORS

LIMITING INDEX-FINGER FORCE

ABSTRACT

Surgical reconstruction of the hand often targets restoration of tip and key pinch, which involves the generation of force by the thumb and the index finger in a specific finger/thumb posture. We report muscle coordination patterns associated with production of maximal force by the index-finger at the distal phalanx in three orthogonal directions. Statistical analysis of EMGs from all seven finger muscles classified the muscles into distinct functional excitatory groups ($p<0.05$). For palmar force (perpendicular to distal phalanx; 24.5N adjusted mean ±0.58SE) all muscles were highly excited, except palmar interosseous was silent. For distal force (colinear with the distal phalanx; 22.3N±0.58) the interossei were excited six times higher, and the flexors and lumbrical four times higher than the extensors, which were silent. For lateral force (in radial direction; 12.7N±0.58), extensor communis was excited three times higher than flexor superficialis, which was silent; extensor indicis and palmar interosseous were the second most excited; flexor profundus and lumbrical the second least excited; and dorsal interosseous was excited at the middle level. A 3-dimensional, 7-muscle model of the finger reproduced the force and coordination observed with palmar and distal force generation. However, interossei co-excitation observed in lateral force production could not be replicated. Analysis of the model showed that palmar force is most sensitive to flexor moment arms at the proximal interphalangeal joint, distal force to dorsal interosseous force production, and lateral force to extensor force production.

INTRODUCTION

The functional outcome of surgery to restore grasping varies (McFarlane, 1987; Hentz, *et al.*, 1988; Hentz, *et al.*, 1992). Because patients can coordinate muscles to utilize postoperative finger musculoskeletal structure (Leffert and Meister, 1976; Moberg, 1990), musculoskeletal, rather than neural, factors seem to bound grasping performance. Thus, an understanding of musculoskeletal function of the fingers and thumb is essential.

Biomechanical models have successfully identified musculoskeletal factors crucial to surgical restoration of lower extremity (Delp and Maloney, 1993) and hand function (Spoor, 1983; An, *et al.*, 1985; Thompson, *et al.*, 1988). Identifying factors limiting static index-finger forces essential for tip and key pinch, two grasping modalities targeted for surgical restoration, still remains a challenge.

Index-finger models have been restricted in their ability to explore surgical factors in detail because of inadequate representation of the kinematics and muscles. Models have either reduced the number of independent muscles (Weightman and Amis, 1982), or set some muscle forces to zero (An, *et al.*, 1979; Weightman and Amis, 1982; An, *et al.*, 1985; Harding, *et al.*, 1993). Sagittal plane models (Weightman and Amis, 1982; Spoor, 1983; Lee and Rim, 1990; Harding, *et al.*, 1993) can be used to study neither laterally directed forces (as in key pinch) nor the muscle coordination necessary to retain the finger neutrally abducted while it generates a finger output torque (the distal phalanx can exert a finger output torque in the sagittal plane independently of finger force). Conversely, complex models are generally statically indeterminate and cause ambiguity in the muscle excitation pattern producing a given finger force (Chao and An, 1978). Nevertheless, unique excitation patterns are predicted during generation of maximal finger forces, regardless of the complexity of the system (Chao and An, 1978; Spoor, 1983; Gordon, 1990; Kuo and Zajac, 1993). The computational demands of these geometric methods has precluded their application to finger models with more than one degree of static indeterminacy.

Published intramuscular electromyograms (EMGs) recorded during index-finger force production (Close and Kidd, 1969; Long, *et al.*, 1970; Maier and Hepp-Reymond, 1995a) have limited usefulness to the verification of model-generated unique excitation patterns. No study has simultaneously recorded EMGs from all seven index-finger muscles during maximal finger force production. Furthermore, force measurement techniques may confound the interpretation of EMGs because the compliant and high-friction interface between the finger pad and dynamometer allows much latitude in the direction of force application and finger output torque is not measured. Also, finger (Weightman and Amis, 1982; Mathiowetz, *et al.*, 1985) and wrist (O'Driscoll, *et al.*, 1992) posture affects finger mechanics and muscle fiber length, which affects muscle force and EMG output (Zajac, 1992). Such factors may explain the variation in measured maximal tip and key pinch forces (19 to 106 N (Weightman and Amis, 1982; An, *et al.*, 1985)) and EMG patterns (Close and Kidd, 1969; Long, *et al.*, 1970; Maier and Hepp-Reymond, 1995a).

In this study, we computed the unique muscle excitation patterns associated with maximal index-finger force production by applying a generalized geometric method to a 3D, seven-muscle finger model with three degrees of static indeterminacy. We recorded EMGs from all muscles of the finger in eight subjects exerting maximal force in three precisely-controlled directions. Comparison of model-generated forces and excitation patterns with measurements identified musculoskeletal factors limiting index-finger force production.

9

MATERIALS AND METHODS

Eight subjects (27 ± 6 (SD) yrs) were instructed to produce maximal force three times in each of

five randomized directions (palmar, distal, lateral, dorsal and medial) while maintaining the finger

flexed and the wrist extended (Figure I.1). Dorsal force is opposite to palmar, and medial force

opposite to lateral. The finger posture chosen required that active muscle forces, rather than

passive muscle forces (Keir, *et al.*, 1996) or joint structures (Tubiana, 1981), dominate the

production of joint torques. Two other finger postures (Table I.6, top; postures were randomized

with force directions randomized at each posture) were also studied, but this report emphasizes

the results for palmar, distal and lateral forces when the finger is most flexed because of their

importance to functional tasks (e.g., key and tip pinch).
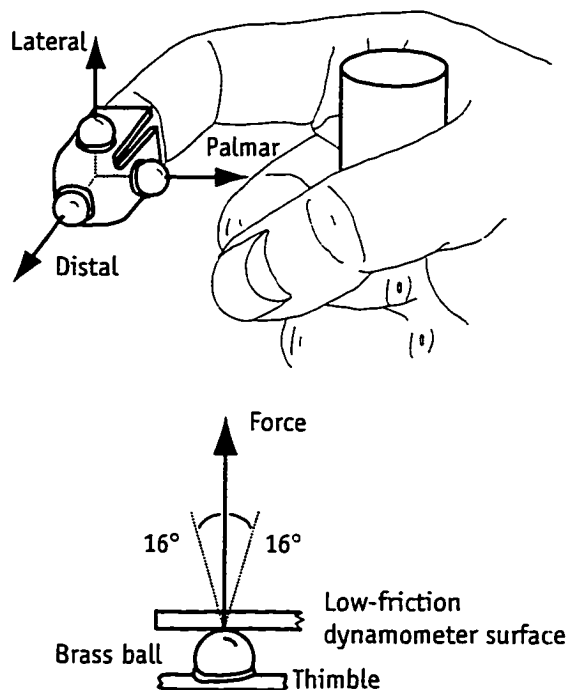
FIGURE I.1. Task constraints in the generation of finger force.
Subjects wrapped their dominant right hand around a fixed dowel and generated maximal index finger force in the palmar, distal and lateral directions while maintaining a standard posture (finger in neutral ad-abduction, 45° flexion at metacarpophalangeal and proximal interphalangeal joints, and 10° flexion at distal interphalangeal joint; wrist in 80° extension and neutral radial deviation; index not resting against middle finger). Subjects wore custom thimbles with 5mm brass balls. Finger force had to be directed within 16° of the surface normal for the ball in contact not to slip. Finger output torque had to be zero for the ball not to rotate.

FIGURE I.2. Robot arm holding force sensor. A 3-axis dynamometer (0.1 N resolution in all axes) was positioned and rigidly held by a 6-DOF Unimate Puma 200 robot such that one ball at a time come in contact with the low-friction surface of the dynamometer.

Each subject wore a tight-fitting thimble molded to the contour of her/his finger (Figure I.1 and Figure I.2). The embedded balls in the thimble ensured low-friction contact against the dynamometer (to assure the force is directed perpendicular to the sensor surface) and no generation of "finger output torque" (the distal phalanx of the index-finger can produce both force and a torque in the sagittal plane, i.e., finger output torque). The instructions to each subject were to increase force magnitude (a trace on a computer screen) beyond the previous maximum (a reference line on the screen) while maintaining the posture. A preliminary trial provided the first maximum for each force direction. Sufficient time between trials (at least 30 s) prevented fatigue (Enoka and Stuart, 1992). Trials in which static posture was not maintained were repeated. In a second session the following day, in addition to force, EMGs from fine-wire intramuscular electrodes in the seven muscles of the index-finger (Burgar, *et al.*, 1996; Appendix A) were recorded (Figure I.3). Maximal force and the muscle excitation pattern were defined as the average force and the average EMG pattern in a 750 ms window centered on peak force (Figure I.3). Each EMG was

11

normalized by the value recorded during separate trials where each muscle was held isometric

during maximal voluntary contraction. From each session, only the trial with the largest peak force

in each direction was used in the analysis. This study was approved by the Institutional Review
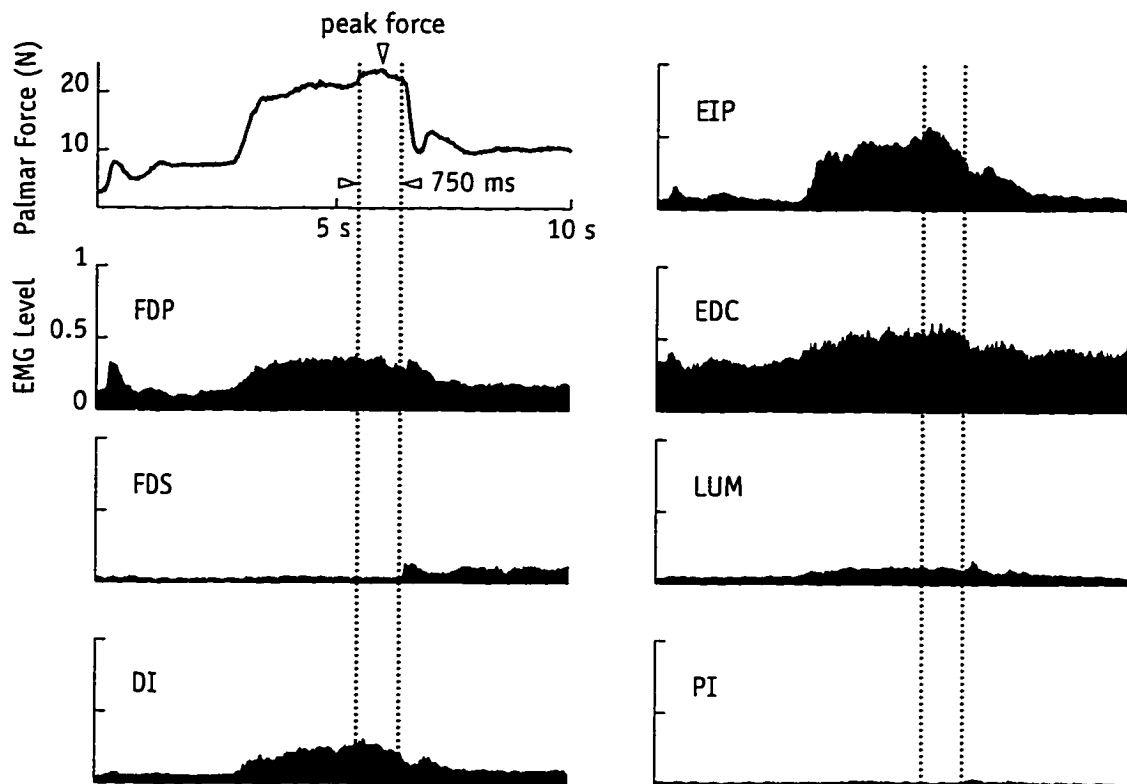
FIGURE I.3. Sample trial (10 s duration).

Palmar force and fine-wire intramuscular electrode recordings from the seven muscles of the index-finger. Standard approaches were used to record from extensor indicis proprius (EIP) and first dorsal interosseous (DI) (Delagi, *et al.*, 1981). Novel approaches were developed to record from first lumbrical (LUM), first palmar interosseous (PI) and the index-finger slips of flexor digitorum profundus, flexor digitorum superficialis and extensor digitorum communis (FDP, FDS and EDC, respectively) (Burgar, *et al.*, 1996; Appendix A). Only 4 of 56 electrode placements were unsuccessful. We were unable to obtain FDP and FDS signals without cross-talk from middle finger flexor muscles in one subject. Two PI electrodes failed in separate subjects (one deteriorated to a weak signal in mid-experiment; the other had cross talk from the adjacent second dorsal interosseous muscle). EMGs (100Hz-20kHz band-pass filtered, amplified, full-wave rectified and smoothed, $\tau = 20$ms) recorded in each trial were normalized by the value obtained during separate maximal isometric voluntary contractions of each muscle. These contractions were performed immediately before and after force production while the investigator braced the finger in the standard posture. In each trial, under concurrent visual feedback, subjects sequentially developed moderate, maximal and moderate force. The force and normalized EMG signals were each averaged over 750 ms centered on peak force. Normalized EMG levels below 0.15 were indistinguishable from baseline noise and graded silent.

Board (Medical Committee for Protection of Human Subjects in Research) at Stanford University. Each subject read and signed a consent form prior to participation in this study.

The model contains a fixed metacarpal and three phalanges with four degrees-of-freedom (DOFs) (Figure I.4A), seven muscles driving inextensible tendons, and a radio-ulnarly symmetric extensor mechanism. Moment arms are based on measurements from a single fresh cadaver (An, *et al.*, 1983) (Table I.1 & Table I.2). The extensor mechanism model is based on Winslow's tendinous rhombus (Zancolli, 1979) with the vectorial distribution of force between the diagonal and lateral bands dependent on finger posture (Figure I.5). The model of DI inserts into the proximal phalanx exclusively (Tubiana, 1981; An, *et al.*, 1983; Ikebuchi, *et al.*, 1988; Brand and Hollister, 1993) (Figure I.4 B). The effect of interconnections among extrinsic tendons (Fahrer, 1971) to the different fingers were not included.

Isometric force production by each muscle was modeled by scaling its maximal force f_o by excitation level e ($0 \leq e \leq 1$) using a generic muscle model (Zajac, 1989). Nominal f_o values were derived from published physiological cross section areas (PCSAs (An, *et al.*, 1985), Table I.1) and maximal muscle stress ($30 \, \text{N/cm}^2$ (Zajac, 1989)). Muscles were assumed to be at optimal fiber length, with pennation angles (Jacobson, *et al.*, 1992; Lieber, *et al.*, 1992) low enough not to affect f_o (i.e., $< 10°$ (Zajac, 1989)). Reducing the PCSA was considered analogous to placing the muscle in a less advantageous location in its force-length curve (See "Implication 3: Indirect determination of muscle optimal fiber length" on page 50).

The distal phalanx of the index-finger can produce force in three orthogonal directions and a finger output torque. The static properties of the nominal musculoskeletal model are contained in a 4x7 matrix **M** (Equation 1), which maps a 7 element vector $\underline{e} = \{e_{FDP}, e_{FDS}, e_{EIP}, e_{EDC}, e_{LUM}, e_{DI}, e_{PI}\}^T$ (i.e., muscle excitation pattern) into a 4 element vector $\underline{ft} = \{palmar\ force, distal\ force, lateral\ force, finger\ output\ torque\}^T$(i.e., finger tip force/torque, Figure I.4)

13

$$\underline{ft} = \mathbf{M}\,\underline{e} \tag{EQ 1}$$

$$\mathbf{M} = \mathbf{J^{-T}RF_0} \tag{EQ 2}$$

where $\mathbf{J}$ is the 4x4 Jacobian of the three-phalanx/four-DOF finger, $\mathbf{R}$ the 4x7 moment arm and

extensor mechanism interaction matrix, and $\mathbf{F_0}$ the 7x7 diagonal matrix of nominal f_0 values.

Extensor mechanism interactions define the distribution of EI, EC, PI and LUM forces at the

interphalangeal joints (Figure I.5). $\mathbf{M}$ is a function of 45 anatomical parameters: 3 phalanx lengths,

28 moment arm values (4DOFs x 7 muscles), 3 extensor mechanism parameters and 7 PCSAs.

These parameters were defined as either independent (Table I.1), dependent (Table I.2) or fixed

(Table I.2). Independent parameters were arbitrarily defined as those that are either posture

dependent (e.g., moment arms), assumed (e.g., extensor mechanism force distribution), or

estimated (e.g.,PCSAs). For a given finger posture, $\mathbf{M}$ is a constant *non-invertible* matrix, i.e., several

$\underline{e}$ produce a given $\underline{ft}$.

A

B
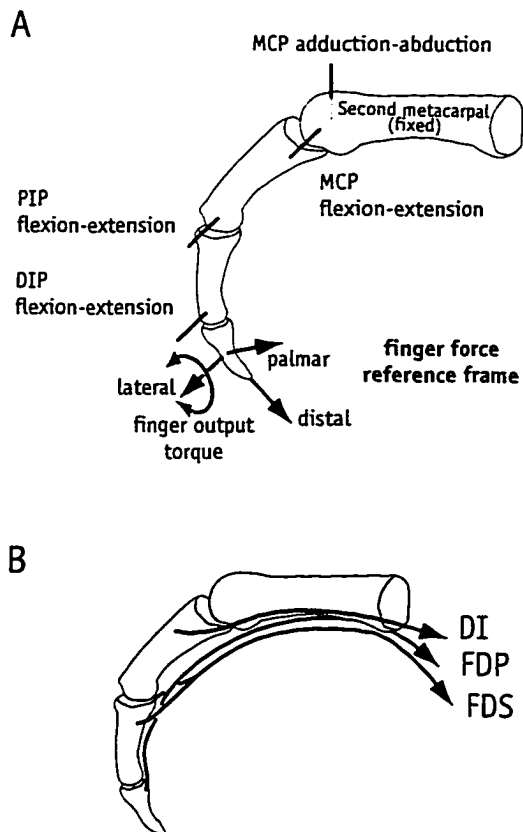
FIGURE I.4. Index finger model.
(A) Four DOFs are assumed between the fixed metacarpal and three phalanges: two perpendicular hinges (ad-abduction and flexion-extension at the metacarpophalangeal joint (MCP) (Youm, et al., 1978b)) and a single flexion-extension hinge at the proximal and distal interphalangeal joints (PIP and DIP, respectively) (An, et al., 1979). The finger force reference frame for the three mutually perpendicular forces (palmar, distal and lateral) is fixed to the distal phalanx. Because of the presence of three flexion-extension hinges, the distal phalanx can control a torque in the sagittal plane (i.e., "finger output torque") independently of finger force. (B) The tendon paths of the DI, FDP and FDS are shown (see Figure I.5 for paths of the other four musculotendinous units)

14

Winslow's Tendinous Rhombus

A

B
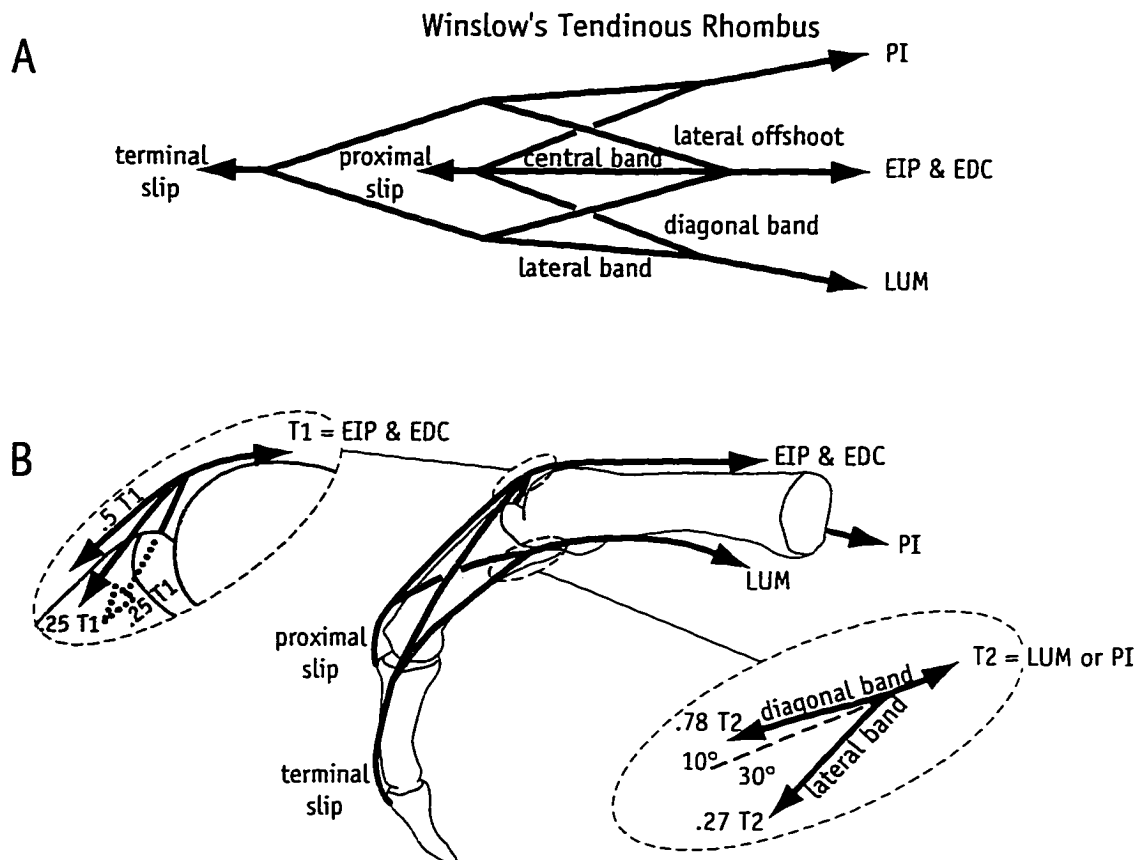
FIGURE I.5. Extensor mechanism model.

A radio-ulnarly symmetric adaptation of Winslow's tendinous rhombus (Zancolli, 1979) is used. (A) Tendons from the EIP and EDC, PI and LUM combine to form the proximal and terminal slips, which have extensor moment arms at the interphalangeal joints (Table I.1). (B) The central band and each lateral offshoot from EIP and EDC were nominally assumed to receive one-half and one-quarter of the tension (T1) in the combined extensor tendon, respectively. The bifurcations of LUM and PI tendons (T2) into the diagonal and lateral bands (known to change with finger posture (Garcia-Elias, et al., 1991)) are considered nodes of a flat net in static equilibrium where the tension in each band depends on their relative orientation. The angles of the diagonal and lateral bands with respect to the proximal tendon were nominally set to 10° and 30°, respectively. Tensions in the proximal and terminal slips were assumed to be algebraic sums of the tensions in the bands and offshoots.

The unique $\underline{e}$ producing the maximal biomechanically feasible magnitude of a given $\underline{ft}$ (Chao

and An, 1978; Spoor, 1983; Gordon, 1990; Kuo and Zajac, 1993) was computed. Geometrically, a

muscle excitation pattern specifies a point in 7D excitation space, and all possible excitation

patterns lie inside a 7D unit hypercube ($0 \leq e_{FDP}, e_{FDS}, e_{EIP}, e_{EDC}, e_{LUM}, e_{DI}, e_{PI} \leq 1$). Computational

geometric principles (Avis and Fukuda, 1992) were applied to 7D space to find the subset of the

unit hypercube containing all possible excitation patterns producing zero finger output torque

(consistent with the experimental task). The extreme points of this subset were mapped through **M**

to produce a convex 3D polyhedron (Chvátal, 1983) in finger force/torque space whose surface, by

construction (Chao and An, 1978; Spoor, 1983; Gordon, 1990; Kuo and Zajac, 1993), represents the

limits on achievable static forces (i.e., $\underline{ft}$ with zero finger output torque, Figure I.6). Thus, a point on
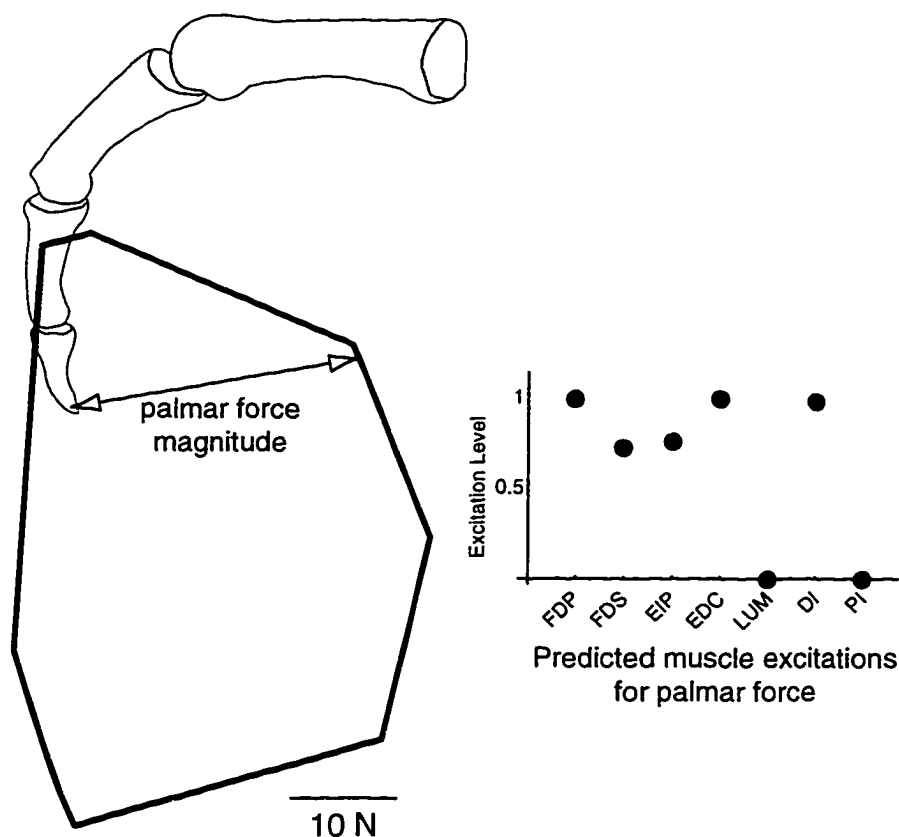
FIGURE I.6. Achievable force polyhedron in the plane of finger flexion.
The boundary specifies the limits on static forces without finger output torque. The maximal magnitude
of force in the palmar direction is the distance between the finger tip and the boundary in the palmar
direction. The muscle excitations that produce every maximal force is known.

16

the surface of this 3D polyhedron corresponds to a unique excitation pattern, and the distance to

the origin specifies the maximal biomechanically achievable magnitude for that force (See

"Appendix C: Sample calculation of feasible force set of point-forces in the plane of finger

flexion").

TABLE I.1. Independent model parameters

	Joint	Tendon	Nominal Value	Adjusted Value	Change %
	MCP adduction	FDP	2.90	—	0
	(adduction +)	EIP	0.30	—	0
	(abduction -)	EDC	-1.19	—	0
		LUM	-3.84	-4.61	+20
		DI	-6.77	—	0
Moment arms, mm (An, et al., 1983)		PI	4.08	6.94	+70
	MCP Flexion	FDP	12	9	-25
	(flexion +)	EIP	-7.77	-9.32	+20
	(extension -)	LUM	7	—	0
		DI	2	—	0
		PI	4	—	0
	PIP Flexion	FDP	6.5	5.07	-22
		proximal slip	-2.75	-3.44	+25
	DIP Flexion	FDP	3.64	—	0
		terminal slip	-1.5	—	0
		Item			
Extensor Mechanism		Proportion to proximal slip	50%	62.5%	+25
		Top bifurcation angle	10°	79°	+690
		Bottom bifurcation angle	30°	39°	+30
		Muscle			
		FDP	4.10	—	0
		FDS	3.65	7.3	+100
PCSA, cm² (An, et al., 1985)		EIP	1.12	0.78	-30
		EDC	1.39	3.06	+120
		LUM	0.36	0.72	100
		DI	4.16	—	0
		PI	1.6	4.32	170

Because a lumped parameter model of maximal muscle force production is used, a reduction in PCSA is equivalent to the muscle fibers being in a less favorable location in the f-l curve. An increment in PCSA indicates that the model required greater maximal force from that muscle, suggesting that its experimental PCSA value was underestimated.

17

TABLE I.2. Fixed and dependent model parameters

			Fixed	Proportional to	Rationale
Phalanges	proximal		50 mm		(An, *et al.*, 1979)
	middle		31 mm		ditto
	distal		16 mm		ditto

	Name	**Joint**			
Postures	flexed	MCP	45°		MCP neutrally ad-abducted
		PIP	45°		
		DIP	10°		
	intermediate	MCP	45°		MCP neutrally ad-abducted
		PIP	10°		
		DIP	10°		
	extended	MCP	10°		MCP neutrally ad-abducted
		PIP	10°		
		DIP	10°		

	Joint	**Tendon**			
Moment arms	MCP abduction	FDS		0.5 FDP	(An, *et al.*, 1983).
	MCP Flexion	FDS		1.1 FDP	ditto
		EDC		EIP	ditto
	PIP Flexion	FDS		0.9 FDP *	ditto
		EIP		proximal slip	Winslow's rhombus (Figure 4).
		EDC		proximal slip	ditto
		LUM		proximal slip	ditto
		DI	0 mm		No proximal phalanx insertion (Tubiana, 1981; An, *et al.*, 1983; Ikebuchi, *et al.*, 1988).
		PI		proximal slip	Winslow's rhombus (Figure 4).
	DIP Flexion	FDS	0 mm		No distal phalanx insertion (Tubiana, 1981).
		EIP		terminal slip	Winslow's rhombus (Figure 4).
		EDC		terminal slip	ditto
		LUM		terminal slip	ditto
		DI	0 mm		No distal phalanx insertion (Tubiana, 1981).
		PI		terminal slip	Winslow's rhombus (Figure 4).

* In the extended posture (Table I.6), the PIP moment arm of
FDS is 0.8 FDP

RESULTS

All static finger forces were directed within $4.7° \pm 2.2°$ (SD) of the normal to the dynamometer surface. The presence of intramuscular electrodes did not affect force production ($p<0.46$, repeated measures ANOVA post-hoc pairwise comparisons used throughout). Force magnitudes were different for each direction (Table I.3, $p<0.05$, all pairs).

EMGs were statistically grouped into functional excitatory groups ($p<0.05$, Figure I.7). For palmar force all muscles were highly excited, except palmar interosseous was silent. For distal force the interossei were excited six times higher, and the flexors and lumbrical four times higher than the extensors, which were silent. For lateral force, extensor communis was excited three times higher than flexor superficialis, which was silent; extensor indicis and palmar interosseous were the second most excited; flexor profundus and lumbrical the second least excited; and dorsal interosseous was excited at the middle level.

TABLE I.3. Force magnitudes (N)

Force	Experimental Adjusted Mean ± SE	Nominal Model	Adjusted Model
Palmar	24.5 ± 0.58	13.4	24.2
Distal	22.3 ± 0.58	19.6	38.9
Lateral	12.7 ± 0.58	27.2	32.1

Forces with and without EMG electrodes are combined because there was no significant difference between them ($p<0.46$)

The nominal model underestimated palmar and distal force magnitudes by 45 and 12%, respectively, and overestimated lateral force by 2 times (Table I.3). The nominal model appropriately estimated extensor activity in all force directions, the excitation of muscles within baseline noise, and (for distal force) the high PI activity (Figure I.8). LUM and PI activity were particularly underestimated for palmar and lateral force, respectively. FDP activity was underestimated for all force directions; FDS for palmar and distal forces. After modification of

Force | EMG Groups

Palmar (P)

Lower — P1   Higher — P2

PI .11 | FDS .29 | DI .3 | LUM .32 | EIP .33 | EDC .37 | FDP .4 — Normalized mean EMG

Distal (D)

D1   D2   D3

EIP .07 | EDC .1 | FDS .38 | FDP .43 | LUM .45 | DI .58 | PI .64

Lateral (L)

L1   L2   L3   L4

FDS .14 | FDP .22 | LUM .22 | DI .29 | PI .4 | EIP .41 | EDC .45
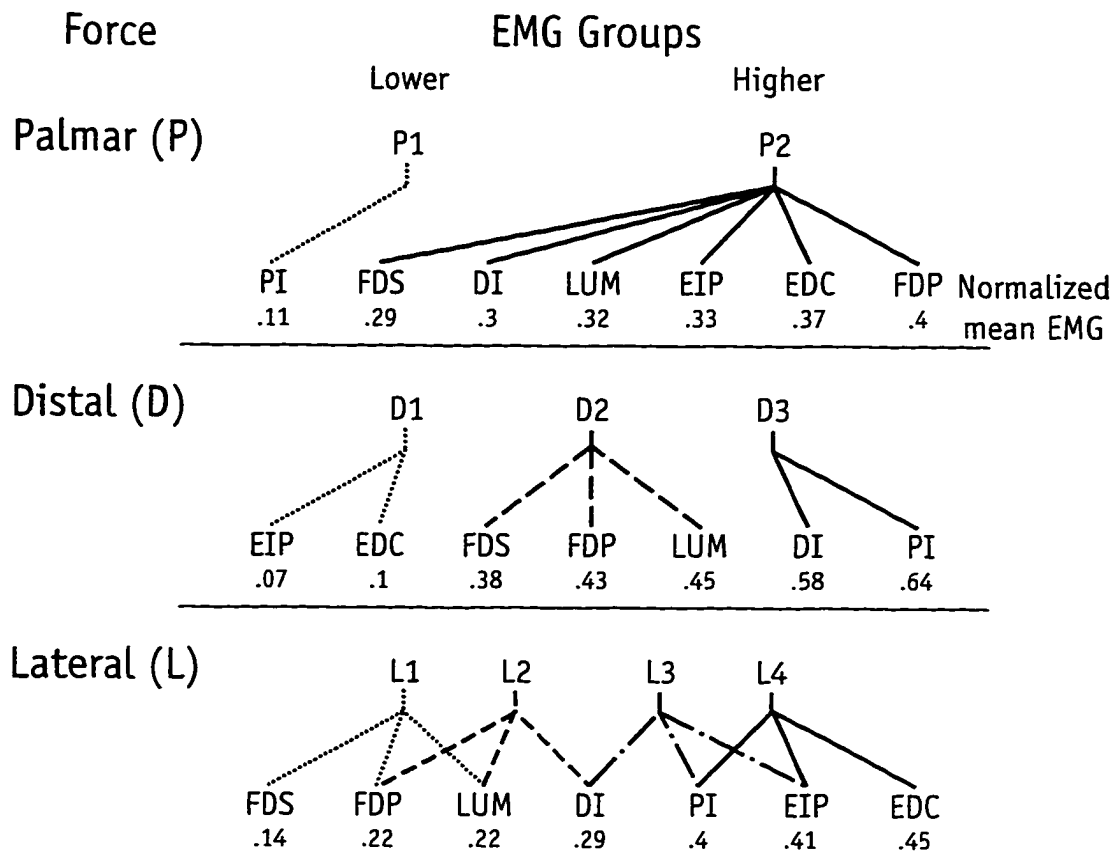
FIGURE I.7. Statistical grouping of muscles by mean normalized EMG level. Repeated measures ANOVA pairwise comparisons, n=8, p<0.05. The seven finger muscles are ranked from left to right by mean normalized EMG level. Muscles can be classified into 2 or 3 distinct functional excitatory groups during generation of palmar and distal force, respectively. For lateral force, no such classification is apparent but, statistically (p<0.05), EDC is the most excited muscle, FDS the least excited and DI is excited at an intermediate level.

only six moment arms (all but one by ≤ 25%) and adjusting five PCSAs (Table I.1), the model reproduced well all force magnitudes (Table I.3) and the major features of the EMG patterns associated with palmar and distal forces (Figure I.9; see Discussion regarding LUM).

Palmar and distal force magnitudes are predicted to be most sensitive to flexor moment arms at the proximal interphalangeal joint and to DI PCSA, respectively (Table I.4). Reasonable adjustments to independent parameters were incapable of reproducing the co-excitation of interossei recorded during production of lateral force (Figure I.9). Since co-contraction is an important feature of lateral force production (see Discussion), we have little confidence in the

Palmar

Distal

Lateral
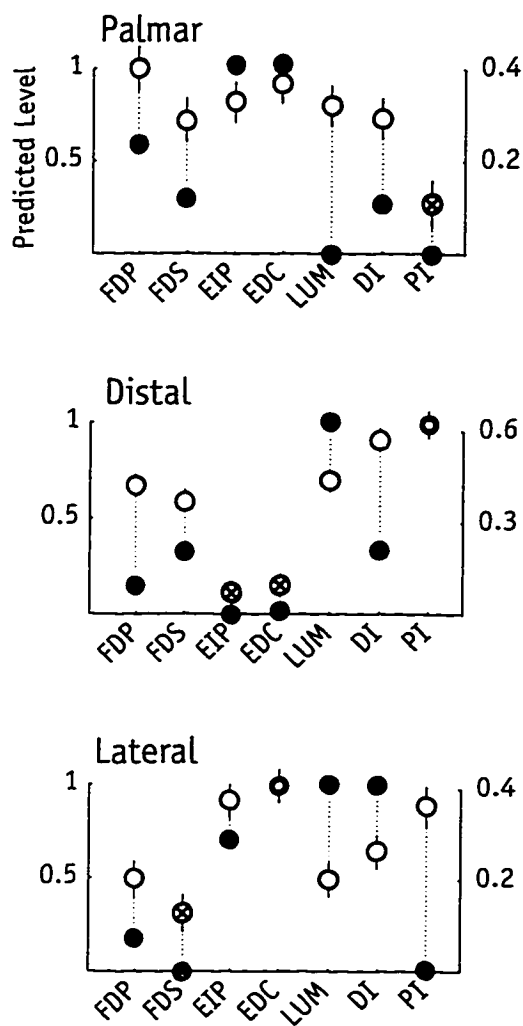
FIGURE I.8. Comparison of mean normalized EMG levels to model-generated excitations.
Open circles denote average normalized EMG levels ± SE (right scale), crossed circles EMGs indistinguishable from baseline noise, filled circles excitation levels predicted by the model (left scale). Separate scales facilitate the comparison of excitation patterns.

model's ability to predict the lateral-force sensitive parameters. Lastly, in contrast with the model-generated excitations spanning a range between zero and 1 (i.e., 100%), normalized EMG levels spanned a range between only zero and 64% (Figure I.7).

The excitation patterns varied with finger posture, except for force generated distally (cf. Figure I.9 with Figure I.10). The model reproduced these observations if moment arms were assumed to change moment between postures (Table I.6) (An, et al., 1983). PCSAs also had to be changed with posture, but these changes are artifactual, a consequence of the lumped parameter muscle force model in which the f-l properties of muscle fibers are not unaccounted for explicitly at present (See "Implication 3: Indirect determination of muscle optimal fiber length" on page 50).

Palmar

Distal

Lateral
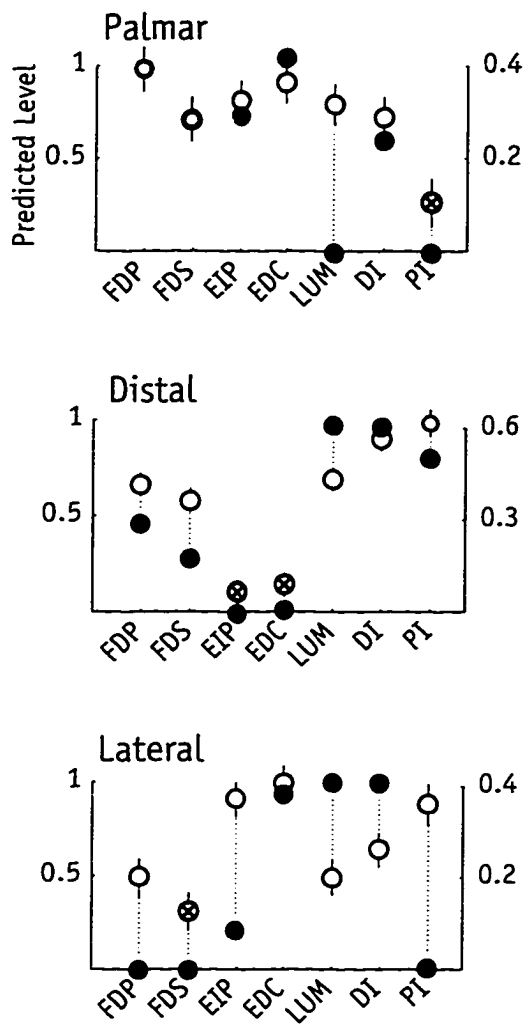
FIGURE I.9. Comparison of mean normalized EMG levels to excitations predicted by the adjusted model.

Six moment arms and five PCSAs were modified (Table I.1). Model excitations for palmar and distal force compare favorably with the experimental data. Reasonable modifications to the independent parameters are incapable of producing co-activation of DI and PI in lateral force.

In essence, the changes in PCSA with posture can be interpreted as muscles having different force production capabilities at different postures because postural changes induce fiber length changes and place muscle fibers in a different location of the f-l curve.

22

TABLE I.4. Relative sensitivity of force magnitudes to independent model parameters

	Joint	Tendon	Palmar	Distal	Lateral
Moment arms, mm	MCP adduction (adduction +) (abduction -)	FDP EIP EDC LUM DI PI	— — — — — —	-0.21 — — — 0.77 -0.67	— — 0.11 0.11 0.94 —
	MCP Flexion (flexion +) (extension -)	FDP EIP LUM DI PI	-0.86 0.5 — — —	0.9 — 0.14 0.23 0.37	— — — — —
	PIP Flexion	FDP proximal slip	1 -0.23	-0.9 0.5	— —
	DIP Flexion	FDP terminal slip	0.24 —	0.18 -0.17	— —

	Item	Palmar	Distal	Lateral
Extensor Mechanism	Proportion to proximal slip	-0.21	—	—
	Top bifurcation angle	—	0.5	—
	Bottom bifurcation angle	—	-0.17	—

	Muscle	Palmar	Distal	Lateral
PCSA, cm²	FDP	0.34	—	—
	FDS	—	—	—
	EIP	—	—	—
	EDC	0.16	—	—
	LUM	—	0.29	0.14
	DI	—	1.	1.
	PI	—	—	—

The relative sensitivity of an output force **A** to a parameter **P** was calculated by the ratio:

$$\frac{\delta A/A}{\delta P/P} \quad (\text{Kuo, 1987})$$

The table shows the sensitivities normalized by column for the adjusted model.

"—" indicates relative sensitivity is below 0.10.

Because we lump all excitation-independent muscle force parameters as PCSA (i.e., optimal fiber length is assumed, Chapter III), sensitivity to PCSA also means that maximal force following reconstructive surgeries is sensitive to tendon resting length. Because the model cannot reproduce interosseous muscle co-excitation for lateral force, the predicted sensitivities for lateral force may not apply.

23

DISCUSSION

Muscle excitation patterns during the production of low forces were not studied. Furthermore, our model of the extensor mechanism addresses its force distribution function only (cf. studies of tendon excursion (Storace and Wolf, 1982; Leijnse and Kalker, 1995)). Lastly, because we have studied the index finger in mechanical isolation, we have not considered the muscle synergies that may be present during coordination of multiple fingers in grasp.

Though the ball impregnated thimble intentionally forced our subjects to exert direction-specific forces, this design probably did not allow them to exert maximal forces because of the precariousness of the task (try pressing a thumb tack into a low-friction impenetrable surface with maximal force). Also, the thimble loosened somewhat with finger pad compression during palmar and lateral force generation and pushed against the finger nail during distal force production. In fear of thimble movement and discomfort, therefore, subjects may have avoided generating maximal force, which has, at times, been reported to be higher (Weightman and Amis, 1982; An, *et al.*, 1985), in spite of concurrent force feedback (Graves and James, 1990) to our subjects. This may be exemplified by the apparent overestimation of distal force by the model (Table I.3), which is predicted to be inherently greater than palmar force (Chapter II; Valero-Cuevas, 1997), but is particularly precarious to produce. The less than maximal EMG signals recorded in this study support this assertion. Nevertheless, because the recorded forces in the palmar and distal directions and the EMG patterns agree with the model generated ones (after parameter adjustment, Figure I.9; Table I.3; see Discussion below), we assert that the unique, direction-specific excitation pattern that should accompany maximal force generation was indeed used by our subjects, though scaled down as they produced less than maximal force.

The conflicting reports of others of zero (Weightman and Amis, 1982) and substantial (Close and Kidd, 1969) extensor activity during tip pinch may be due to finger force being directed

24
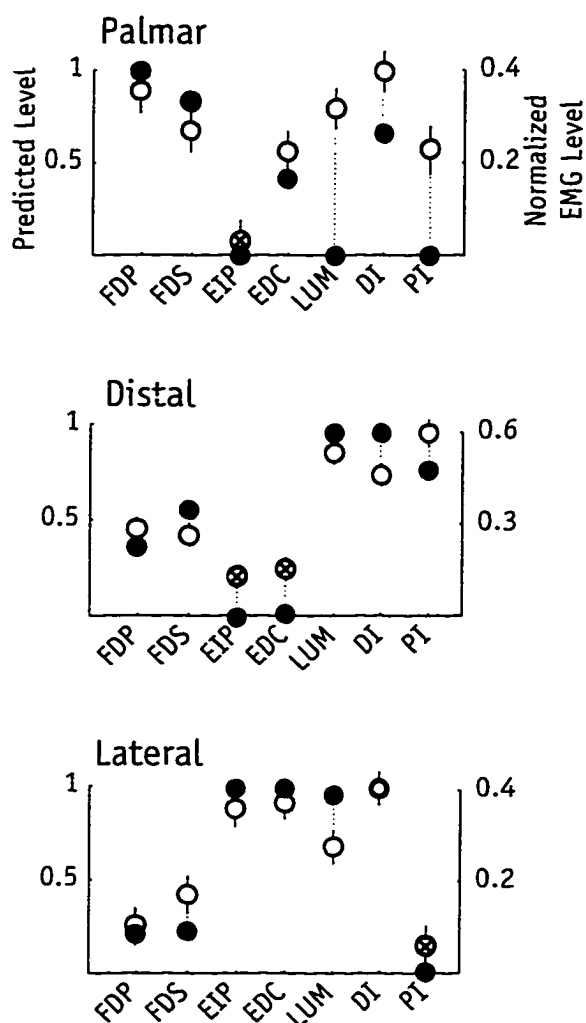
FIGURE I.10. Comparison of mean normalized EMG levels to model-generated excitations, extended finger posture.

Finger is in neutral ad-abduction, 10° flexion at all joints; wrist in 20° extension and neutral radial deviation; index not resting against middle finger. Model parameters change from the flexed posture as shown in Table I.6. Posture order was randomized during data collection. Excitation pattern for distal force is robust to change in posture (c.f. Figure I.9). Patterns for palmar and lateral forces are affected by posture. There is no PI activity during lateral force as the task is mostly one of abduction in this posture.

differently in each of their experiments. In contrast, the thimble and apparatus used in our experiments assured that subjects would generate force in a well-defined direction. We found extensor activity to be very high when palmar force was generated but absent during generation of distal force (cf. EIP & EDC in palmar and distal directions, Figure I.9). Such differences were predicted by the model as well (Figure I.9). Finger and wrist posture was also carefully set in each subject to reduce variability in the location on the f-l curve where the muscle fibers operated (Zajac, 1992).

We believe the modifications of the five PCSAs and six moment arms (all but one by ≤ 25%; Table I.1) in the nominal model are justified. First, these changes were able to reproduce

reasonably well the forces and EMG patterns recorded in all five directions in each of three

postures (Figure I.10; see Appendix B for additional data). Second, reported PCSAs vary much

(Table I.5) and no large change in muscle stress is justified (Zajac, 1989). However, it is very likely

that PCSA s are, in general, underestimated as subjects generated the force magnitudes predicted

by the model without using maximal excitations. PCSA data typically come from older, sometimes

emaciated, cadavers (An, 1996), which may result in underestimation of PCSAs. Third, the

constant-tension method used to measure moment arms (An, et al., 1983) may underestimate those

for PI and LUM as they insert into the sides of the extensor mechanism complex, and may be

tension dependent. At both interphalangeal joints, the flexor moment arms were reduced by about

20%, and the extensor moment arms increased by about 20%, suggesting a slight bias in their

estimation. Although other moment arm values may also need adjustment, the model was not as

sensitive to their values (Table I.4) and were not modified.

TABLE I.5. Comparison of published PCSA values (cm^2)

	(An, et al., 1985)	(Jacobson, et al., 1992; Lieber, et al., 1992)
FDP	4.10	1.77
FDS	3.65	1.71
EIP	1.12	0.56
EDC	1.39	0.52
LUM	0.36	0.11
DI	4.16	1.5
PI	1.6	0.75
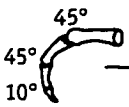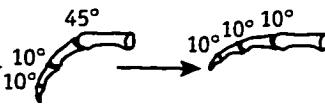
A seemingly major difference between predicted and measured LUM excitation during

palmar force (Figure I.9) is believed to be in actuality minor. Differences in LUM excitation are

meaningless because the model shows low sensitivity of palmar force to LUM parameters

(Table I.4), a consequence of its very low force (Table I.1).

The model does not predict co-excitation of interossei for lateral force because it would reduce

net abduction torque, thus lateral force is overestimated (Table I.3). In contrast, no PI activity was

recorded or predicted in the extended finger posture (Figure I.10) and lateral force magnitude was

predicted within 3 N (Appendix B).

TABLE I.6. Percent Change in independent parameters between postures

	Joint	Tendon	Flexed to Intermediate	Intermediate to Extended
Moment arms, mm	MCP adduction (adduction +) (abduction -)	FDP	0	0
		EIP	0	0
		EDC	0	0
		LUM	0	0
		DI	0	0
		PI	0	0
	MCP Flexion (flexion +) (extension -)	FDP	0	-20
		EIP	0	0
		LUM	0	0
		DI	0	+80
		PI	0	-60
	PIP Flexion	FDP	-10	0
		proximal slip	-20	0
	DIP Flexion	FDP	0	0
		terminal slip	0	0

	Item	Flexed to Intermediate	Intermediate to Extended
Extensor Mechanism	Proportion to proximal slip	0	+20
	Top bifurcation angle	-23	0
	Bottom bifurcation angle	+10	0

	Muscle	Flexed to Intermediate	Intermediate to Extended
PCSA, cm^2	FDP	0	0
	FDS	+25	0
	EIP	+43	0
	EDC	+14	0
	LUM	0	0
	DI	+10	0
	PI	-33	+50

Intermediate posture: 45° flexion at metacarpophalangeal and 10° flexion at both interphalangeal joints; wrist in 45° extension. Extended posture: 10° flexion at all joints; wrist in 10° extension. All postures with finger in neutral ad-abduction, index not resting against middle finger, wrist in neutral radial deviation. Only one finger joint angle changes between consecutive postures. Wrist posture was adjusted to reduce variability in extrinsic muscle EMG.

27

However, the inability of the model to excite PI during lateral force generation in the flexed posture is significant. When the model is constrained to co-excite the interossei, however, abduction torque and lateral force are naturally reduced. Model and experimental agreement of radial force magnitude then occurs (cf. Table 3 with no co-excitation). When no coexcitation is predicted (e.g., lateral force in extended posture, Figure I.10), forces agree to within 3 N (Appendix B).

The co-activation of interossei for lateral force in the flexed posture may be an injury prevention strategy. Finger flexion increases the tendency of lateral force to pronate the proximal phalanx, which our 2DOF MCP model assumes to be passively resisted by joint structures (Youm, *et al.*, 1978a). In reality, the MCP offers limited supination-pronation (Minami, 1985), which Long proposed was actively controlled by the intrinsic muscles (Long, *et al.*, 1970). An analysis of MCP kinematic descriptions (Chapter II) suggest, however, that adding supination-pronation to the model severely compromises lateral force production. Tilting the ad-abduction axis of the 2DOF model (Brand and Hollister, 1993) causes the MCP to be placed in the vulnerable position where passive joint structures become entirely responsible for resisting key pinch force when the finger tip crosses the tilted axis. Both 2 DOF MCP models will lead to shear and torsional loading on the passive structures of the MCP. Thus, interossei co-excitation may simply be an ancillary strategy to prevent joint damage or disarticulation.

The multiarticular nature of finger muscles, however, naturally leads to joint co-contraction and to finger force production being limited by non-obvious musculoskeletal factors. Joint torques cannot be individually controlled as muscles produce simultaneous torques at all joints spanned. Joint co-contraction invariably results (e.g., flexors and extensors to produce palmar force, Figure I.9). Thus, the force capability of any one highly excited muscle limits force production (e.g., extensors during palmar and lateral forces). Also, force production becomes particularly sensitive

to a few (possibly counterintuitive) moment arms and moment arm ratios (Table I.4). For example,

distal force requires MCP flexion torque to be ten times greater than PIP torque (Table I.7).

Therefore, higher PIP flexor moment arms greatly reduce distal force magnitude (Table I.4)

because flexion torques must increase in specific proportions *at all joints* for distal force magnitude

to increase (Table I.7). Frequent co-contraction increases the average contact forces at the joints and

may contribute to the known high incidence of osteoarthritic degeneration of finger joints (Kelsey,

1984).

TABLE I.7. Normalized proportions of net joint torques (τ) necessary to produce finger forces (ff) in flexed posture ($\tau = J^T ff$)

		Force		
		Palmar	Distal	Lateral
Joint Torques	MCP adduction	0	0	-1
	MCP flexion	1	1	0
	PIP flexion	0.62	0.11	0
	DIP Flexion	0.21	0	0

The posture-dependent vectorial distribution of LUM and PI tension (Figure I.5 & Table I.6)

may be an important characteristic of the extensor mechanism. Vectorial distribution (cf. zero-sum

distribution of tension between diagonal and lateral bands) was critical to achieve the observed

dorsal force magnitude (Chapter III), and necessary to increase the predicted excitation of flexors.

EMGs accompanying the production of maximal voluntary static point-forces compared

favorably with the model-generated theoretically unique excitation patterns for maximal palmar

and distal forces. The model cannot reproduce interossei co-excitation for lateral force using solely

musculoskeletal considerations. Both measured and predicted excitation patterns identify

important consequences of the multiarticular nature of finger muscles to finger force production.

Namely, finger force production naturally result in co-contraction at the finger joints, palmar force

is most sensitive to PIP flexion moment arms, and distal and lateral forces to the maximal force of

DI and extrinsic extensors, respectively.

CHAPTER II: EFFECT OF

METACARPOPHALANGEAL JOINT

KINEMATICS ON INDEX-FINGER FORCE

PRODUCTION

ABSTRACT

The 3-D, 7-muscle model of the index finger in Chapter I uses a 2 degree-of-freedom (DOF) description of the metacarpo-phalangeal joint (MCP) and successfully reproduces experimentally measured finger forces in the sagittal plane of finger flexion and the muscle excitation patterns that produce them. This model is not able to reproduce the co-excitation of interossei muscles recorded during production of finger tip force towards the side of the finger (lateral force) in a flexed finger posture. One explanation may be that the kinematic description of the metacarpophalangeal joint in the model does not include a supination-pronation DOF, which has been proposed to exist in the anatomical joint. However, because excitation patterns must be interpreted within the context of force production, this study compares the force production capabilities of finger models that use three different MCP kinematic descriptions. The model in Chapter I has force production capabilities comparable to those measured experimentally. Using a tilted ad-abduction axis at the MCP results in exceptionally high lateral force predictions in flexed postures, and it is predicted that lateral force is infinite and not controllable in the functional flexed posture where the finger tip crosses the tilted axis. Adding a third supination-pronation DOF severely compromises the inherent capability of the finger to produce lateral force. It is concluded it is unlikely that supination-pronation is an independent kinematic DOF at the MCP. The co-excitation of the interossei may be simply be an injury prevention strategy.

31

INTRODUCTION

The metacarpophalangeal joint (MCP) has been described as simply two perpendicular flexion-extension and ad-abduction hinges (Youm, *et al.*, 1978a) (MCP-1, Figure II.1). Using this MCP description, a 3-D, 7-muscle biomechanical model of the static force capabilities of the index-finger (Model 1) was shown capable of reproducing the experimental magnitudes of maximal finger tip forces (Chapter I). Model 1 can also reproduce the muscle excitation patterns seen in subjects producing finger tip forces in the plane of index-finger flexion (Chapter I). Model 1 can not reproduce the coactivation of palmar and dorsal interosseous muscles seen in subjects producing lateral forces (i.e., forces perpendicular to the sagittal plane of index-finger flexion) in flexed finger postures. This is because the assumed MCP kinematics make the interossei behave as an antagonist ad-abduction pair, whose coactivation can only reduce net ad-abduction torque and lateral force.

Clinically, the MCP is known to allow some supination-pronation of the proximal phalanx, which Long (1970) proposed is controlled by coactivation of the intrinsic muscles. Alternative kinematic descriptions of the MCP with supination-pronation exist. Having the ad-abduction hinge tilted 20° from the vertical (Model 2) (Brand and Hollister, 1993) results in a compound ad-abduction and supination-pronation motion (MCP-2, Figure II.1). Adding a third hinge to Model 1 allows independent supination-pronation (MCP-3, Figure II.1) (Long, *et al.*, 1970; Berme, *et al.*, 1977).

Models incorporating these alternative descriptions of the MCP may predict interossei coactivation during lateral force production. However, recorded muscle excitation patterns must be understood within the context of force production. This study compares the force production capabilities of index finger models adopting each of these MCP kinematic descriptions.

32

METHOD

Joint torques $\vec{\Gamma}$ are related to force/torque $\vec{f}$ at the tip of the finger by the inverse transpose

Jacobian $\mathbf{J}^{-T}$, defined by the kinematics of the finger at each finger posture.

$$\vec{f} = \mathbf{J}^{-T}\vec{\Gamma}$$

$\vec{\Gamma} = \{\tau_1,....,\tau_j\}, j = \text{\# of finger degrees-of-freedom}$

$\vec{f} = \{f_x, f_y, f_z, \tau_x, \tau_y, \tau_z\}$

EQ II.1

Assuming every joint torque vector $\vec{\Gamma}$ of unit magnitude can be generated, the singular value

decomposition (SVD) of $\mathbf{J}^{-T}$ specifies the size and orientation of the manipulating force/torque

ellipsoid (Yoshikawa, 1990). In essence, the SVD of a matrix describes how the magnitude of any

vector multiplied by that matrix will be affected. In the geometric interpretation of SVD, the

distance from the center of the ellipsoid to any point on its surface specifies the magnitude of $\vec{f}$ in
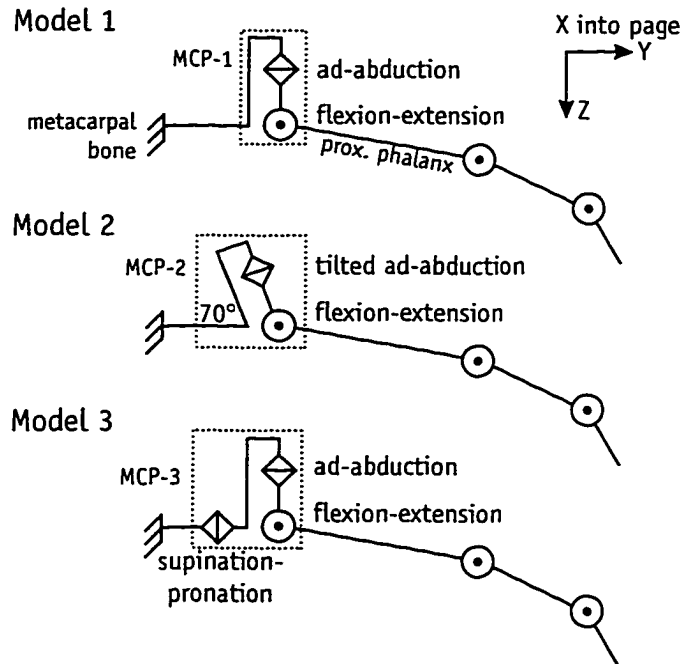
FIGURE II.1. Schematic representation of three kinematic descriptions of the MCP joint.
Model 1 and Model 2 are identical, except for the tilting of the ad-abduction axis in the plane of finger flexion. Model 3 is identical to Model 1 but has an additional supination-pronation axis. For lack of experimental kinematic descriptions of rotation order, we assume ad-abduction and supination-pronation axes are fixed to the metacarpal and do not change orientation with finger flexion.

33

that direction given a unit magnitude input $\vec{\Gamma}$. Thus, the long axis of the manipulating ellipsoid

indicates the direction in which the finger can generate force with the "greatest ease." The short

axis indicates the direction in which the finger has the "least ease" of force production (Figure II.2).
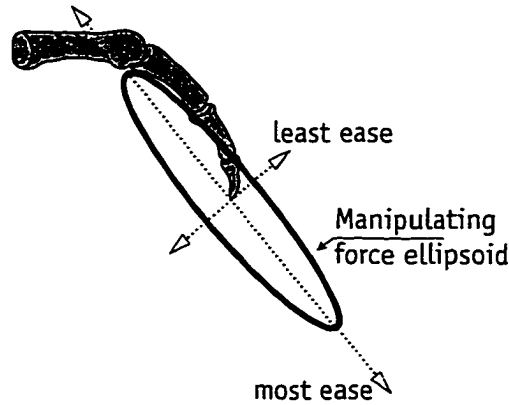
FIGURE II.2. Manipulating force ellipsoid.
The major and minor axes indicate the
directions in which the finger produces the
largest and smallest forces using input joint
torque vectors of equal magnitude.

A 4 DOF index-finger model with three flexion-extension hinges (Figure II.1) can control

torque in the sagittal plane at the distal phalanx (i.e., τ_x or "finger output torque," EQ II.1)

independently of f_x, f_y and f_z forces. Finger forces with zero finger output torque, "point-forces,"

are better suited to the grasping of small and slippery objects and are the subject of Chapter I. For

a joint torque vector $\vec{\Gamma}$ to produce a point-force, it must belong to the nullspace of the τ_x, τ_y and τ_z

rows of J^{-T} because a point-force is defined mathematically as $\vec{f}$ with τ_z τ_y and τ_z (if produced)

equal to zero. The *point-force* ellipsoid can be found by scaling each axis of the force/torque

ellipsoid by the fraction of its corresponding SVD input vector lying in that nullspace. The

distance from the center of the point-force ellipsoid to any point on its surface specifies the

magnitude of the point-force produced in that direction by a unit magnitude $\vec{\Gamma}$.

Force/torque and point-force ellipsoids can also be calculated for a finger model **M** (EQ I.1 and

I.2, on page 14) which maps $\vec{e}$, the 7 element vector of muscle excitations, into $\vec{f}$ .These ellipsoids

forces in plane of finger flexion
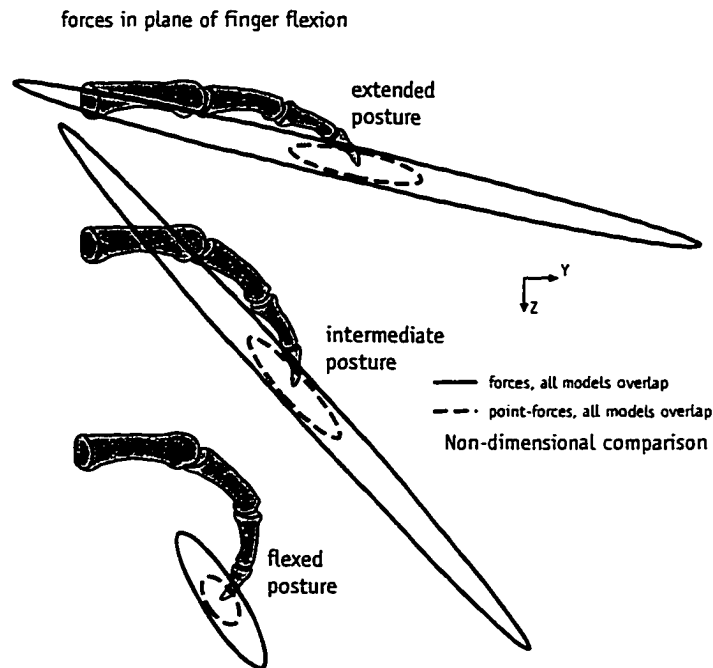
FIGURE II.3. Manipulating ellipsoids in plane of finger flexion for **inverse transpose Jacobians** only. Three MCP models are compared. Ellipsoids without finger output torque constraint (solid lines) and ellipsoids constrained not to produce finger output torque (dashed lines). Introducing point-force constraints reduces the size of the ellipsoids equally for all models.

of **M** indicate the force magnitudes produced by unit magnitude input $\vec{e}$. They differ from the

J^{-T} ellipsoids in that they take into account the strength and moment arms of individual muscles

and the distribution of forces at the extensor mechanism.

The moment arms and extensor mechanism in Models 2 and 3 are assumed equal to those in

Model 1. Tilting the ad-abduction axis on the sagittal plane in Model 2 does not change its moment

arms. The additional supination-pronation moment arms of the intrinsic muscles are assumed

equal to their ad-abduction moment arms. The supination-pronation moment arms of the extrinsic

muscles were set to zero because their tendons paths are parallel to that axis.

RESULTS

The manipulating point-force ellipsoids of J^{-T} indicate that the point-force production capabilities in the plane of finger flexion are equal for all models (Figure II.3). For lateral forces, i.e., in plane perpendicular to finger flexion, Model 2 had greater, and Model 3 had a lesser, lateral force capability than Model 1 (Figure II.4A). Introducing point-force constraints reduces the force capabilities of all models equally in the plane of finger flexion, and similarly for lateral forces (Figure II.3 and Figure II.4B). Increasing finger flexion greatly increases the lateral point-force capability of Model 2.

The shape and orientation of the manipulating force ellipsoids of the models including individual muscle characteristics are similar to the J^{-T} ellipsoids. While all models have comparable sagittal plane ellipsoids, introducing point-force constraints reduces the force capabilities of Model 3 below those of the other two models (Figure II.5). In contrast, Model 3 has the smallest point-force ellipsoids for lateral force in all cases (Figure II.6). At the flexed finger posture, the lateral force capability of Model 2 is also greatly enhanced (Figure II.6).

The magnitude of lateral point-forces measured in Chapter I remain relatively constant as predicted by Model 1, an order of magnitude lower than those predicted by Model 2, and at least 3 times greater than those predicted by Model 3 (cf. Figure II.6B and Table II.1).

TABLE II.1. Lateral force magnitudes, N (±SD)

Posture	+X Force	-X Force
Extended	15 ± 7.6	14.3 ± 8.3
Intermediate	20± 10	14.5 ± 4.5
Flexed	121.6± 9.6	15.2 ± 6.9

Forces with and without EMG electrodes are combined because there was no significant difference between them (p<0.46)

A: lateral forces

B: lateral point-forces
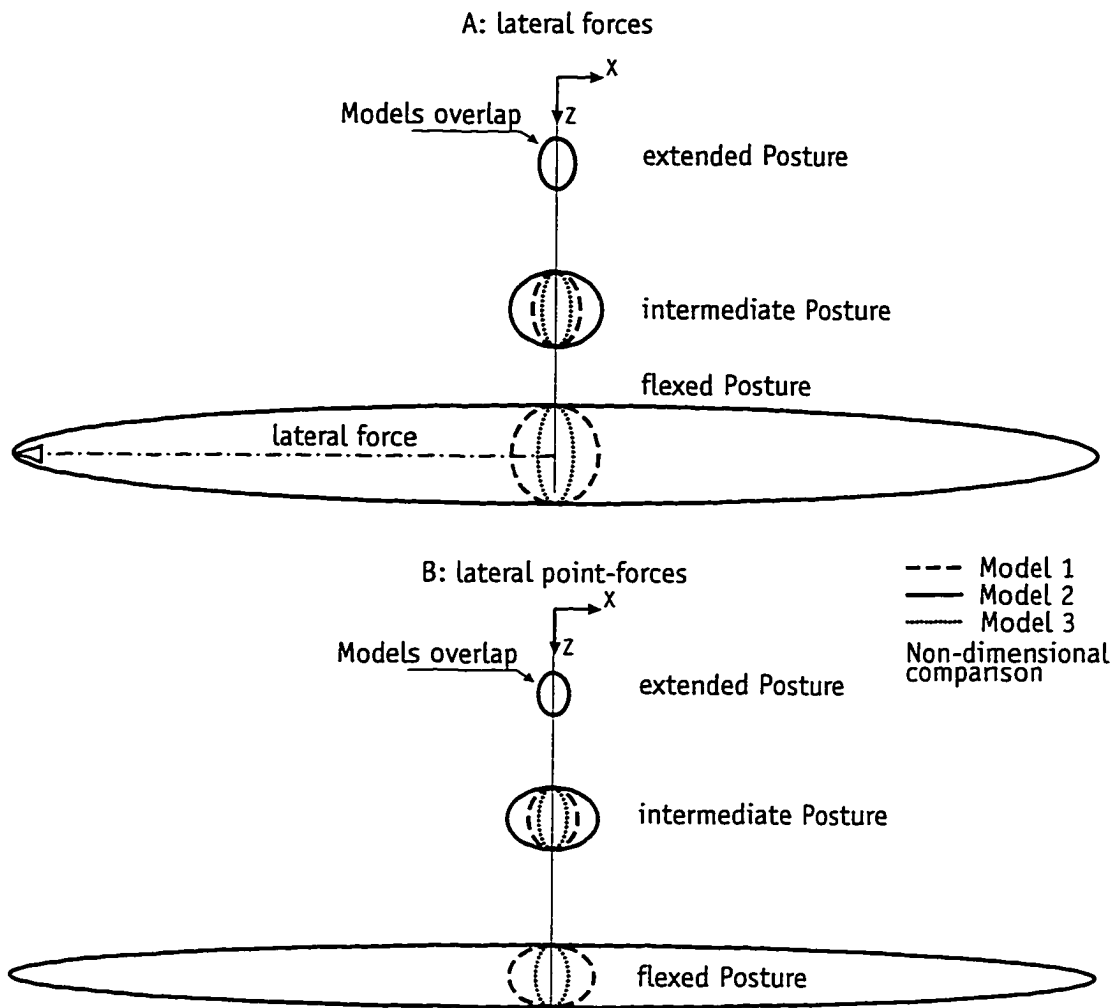
FIGURE II.4. Ellipsoids perpendicular to the plane of finger flexion for **inverse transpose Jacobians** only. Three MCP models are compared. (A) without finger output torque constraint. (B) Constrained not to produce finger output torque. The direction of lateral force is shown.

37

A: forces in plane of finger flexion

B: point-forces in plane of finger flexion

Models 1 and 2 overlap

Models 1 and 2 overlap

Models 1 and 2 overlap

- - - Model 1
—— Model 2
—— Model 3

50 N
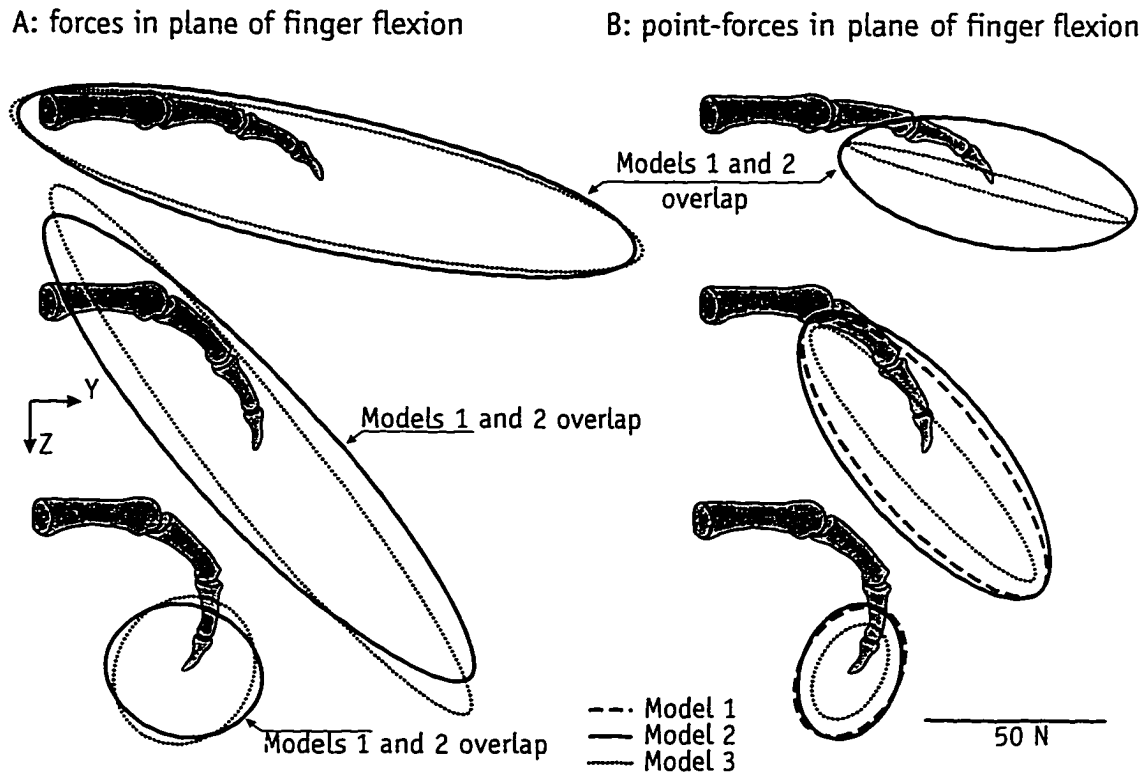
FIGURE II.5. Manipulating ellipsoids in plane of finger flexion for models including musculature. Three MCP models are compared. (A) without finger output torque constraint. (B) Constrained not to produce finger output torque.

38

A: lateral finger forces

extended Posture

intermediate Posture

flexed Posture

B: lateral finger point-forces

--- Model 1
— Model 2
—— Model 3

extended Posture

intermediate Posture

flexed Posture

$$\frac{40\ N}{200\ N}$$
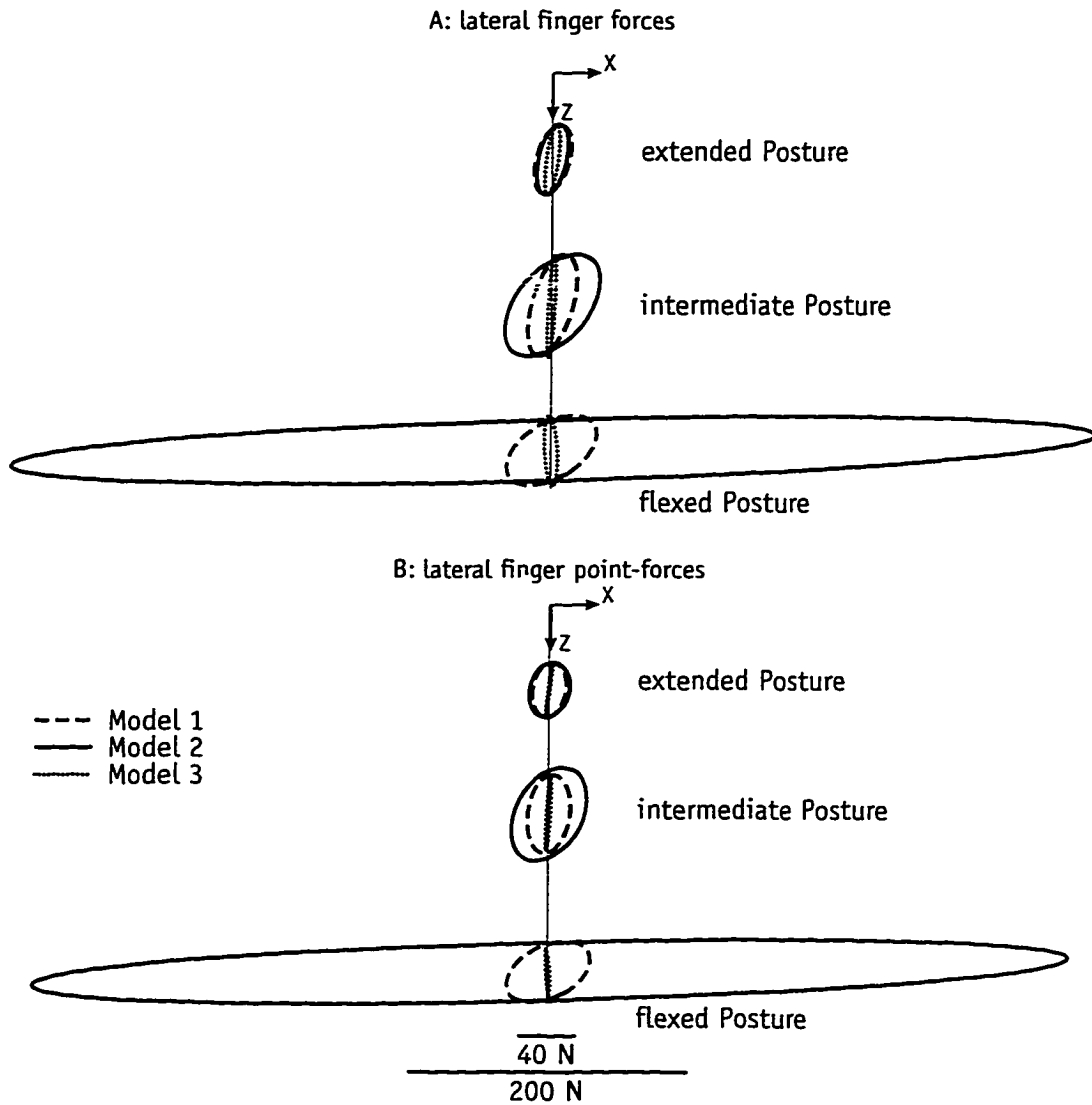
FIGURE II.6. Ellipsoids in plane perpendicular to finger flexion for models including musculature.
Three MCP models are compared. (A) without finger output torque constraint. (B) Constrained not to produce finger output torque. Note similarity to ellipsoids calculated using the inverse transpose Jacobian only (Figure II.4)

39

DISCUSSION

The ellipsoids of the inverse transpose Jacobians underestimate finger force production. The manipulating point-force ellipsoids of a Jacobian reflects how unit-magnitude joint torque vectors, visualized as a sphere, are scaled and rotated by finger kinematics to produce point-forces. This assumes that the finger can generate the same torque magnitude (positive and negative) at all joints. This is not the case for human fingers as some joints are weaker than others, and flexion and extension torque magnitudes may be different in a given joint. Therefore, the ellipsoids of the inverse transpose Jacobians (Figure II.3 and Figure II.4) reflect point-forces produced by torque magnitudes at all joints that are equal to the torque possible at its weakest joint.

The ellipsoids calculated using force and torque production capabilities of individual muscles (Figure II.5 and Figure II.6) overestimate finger force production. Excitation levels are defined to lie between 0 and 1. The manipulating ellipsoid technique assumes that all input excitation vectors of unit magnitude, visualized as a sphere that includes negative excitations, are transformed into finger forces. Because valid unit magnitude excitation vectors define a half-sphere (i.e., positive values only), the true output forces will span a subset of the ellipsoids calculated using a compete input sphere.

MCP kinematics affects force production more than individual muscles characteristics. MCP descriptions lead to particularly different lateral force capabilities in the intermediate and flexed postures, yet the relative shape and orientation of the J^{-T} and M ellipsoids for each MCP description remain similar. The inclusion of the effects of individual moment arms and muscle forces modified sagittal force (cf. Figure II.3 and Figure II.5A) and lateral force ellipsoids (cf. Figure II.4 and Figure II.6A) in all models, with a particularly detrimental effect on the lateral force ellipsoid of Model 3. However, the changes in all models due to these added factors only
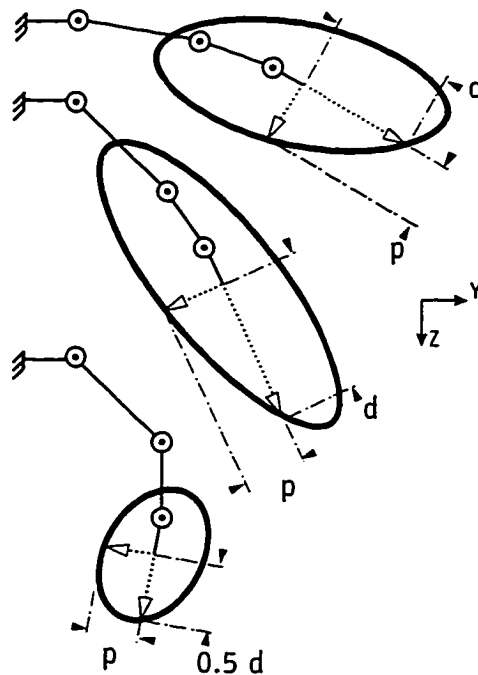
FIGURE II.7. Magnitude comparison of point-forces of Model 1 directed parallel (d) and perpendicular (p) to distal phalanx.

Model 1 has greater distal (d) force capability in the extended and intermediate postures than in the flexed posture. Palmar force magnitude (p) is comparable at all postures.

accentuated the differences in force production among models already created by the different MCP kinematic descriptions.

The kinematics of the finger naturally favor the production of forces parallel to the distal phalanx (corresponding to distal force in Chapter I). The manipulating force ellipsoids in the plane of finger flexion are elongated for all finger Models, particularly in the extended and intermediate postures. Finger flexion, by decreasing the alignment of the phalanges, results in a more even distribution of force production capabilities in the sagittal plane (Figure II.7).

From the force production point of view, it is very unlikely that the anatomical MCP has a true supination-pronation DOF. For the same excitation input, the point-force magnitudes of Model 3 will be smaller than those for Models 1 and 2, and well below experimental values (cf. Figure II.6B and Table II.1).

While Model 2 may be able to produce large lateral point-forces, producing them has the risk of injuring the passive structures that maintain joint integrity. Every finger model gradually looses lateral mobility, and gains lateral force capability, as its finger tip approaches the ad-abduction
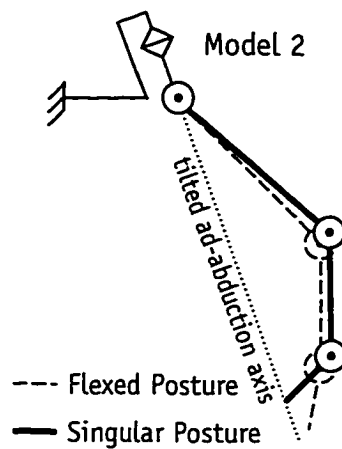
FIGURE II.8. Singular posture for Model 2.

axis. When close to the axis, lateral force production increase dramatically, and becomes infinite

and uncontrollable when reaching the axis (i.e., a singular posture where J becomes non-

invertible (Yoshikawa, 1990)). This loss of controllability in force production is known to

jeopardize the stability of the system (Kuo, 1987). Because the flexed posture is close to the

singular posture (Figure II.8), Model 2 is understandably predicted to produce particularly large

lateral force (Figure II.4). However, the MCP of Model 2 may be vulnerable to damage at the

singular posture because any key pinch forces are resisted by passive joint structures exclusively.

Model 1 has acceptable force production capabilities, but cannot be considered superior to

Model 2 at this point. With Model 1, lateral point-force capabilities increase moderately with finger

flexion (Figure II.6B), in agreement with experimental data (Table II.1). Model 2 is, however, not

invalidated by the fact that experimental lateral forces were not as high as predicted. Subjects may

have simply refrained from producing maximal attainable lateral forces to avoid high shear and

torsional forces at the finger joints, which could lead to injury. Further studies are needed to

establish if index-fingers indeed cannot produce lateral force at the singular posture (Figure II.8).

It is likely the co-excitation of interossei is a strategy to protect the MCP. Lateral finger forces,

besides being produced by joint torques, induce contact shear and torsional forces at the finger

42

joints, and their magnitude is greatest at the MCP. Our models, as idealized kinematic descriptions

of joints, simply assume that joint forces are adequately resisted and that joint disarticulation will

not occur. In reality, it is the passive bone and ligament structures (Berme, *et al.*, 1977; Youm, *et al.*,

1978a; Brand and Hollister, 1993), and possibly interossei coactivation, which prevent the damage

or disarticulation of anatomical joints.

In conclusion, Model 1 or 2 may already be an adequate kinematic description of the MCP.

More complex finger models that include passive joint structures and monitor MCP integrity may

be necessary to elucidate the role of muscle coordination in enhancing joint stability and

preventing injury. However, simpler models suffice to study forces in the sagittal plane of finger

flexion.

CHAPTER III: CLINICAL IMPLICATIONS

IMPLICATION 1: DESIGN OF TENDON TRANSFERS

Finger muscles, whose tendons cross multiple joints, produce simultaneous torques at all joints spanned. At a given finger posture, the proportions among the joint torques (i.e., the torque vector) produced by a muscle's tendon force remain constant because the moment arms at each joint are fixed. Because no two finger muscles have identical tendon paths, each muscle produces a different torque vector with a maximal magnitude proportional to its PCSA. The excitation level of a muscle scales the magnitude of the torque vector between zero and its maximal magnitude.

To produce an index-finger tip force, such as those used for tip or key pinch, finger muscles must together generate a specific torque vector (Table I.7 on page 29). Viewing muscle coordination as the means of combining the multiarticular effects of individual muscles suggests the following approaches to restoring function:

i) Some finger tip force may be restored by transferring a relatively weak muscle

Muscles with intact function are favored as donors for tendon transfers. Because there may be few such muscles available after spinal cord injuries or nerve palsies, the options for tendon transfers are limited. Weak or partially innervated muscles, while available, may not be considered as donors because of their compromised force capabilities.

Judicious use of weak muscles may increase the options for tendon transfers. Consider radial palsy, which removes control over extensor muscles. Extensor muscles are essential to produce lateral force (Chapter I) because they are the only muscles capable of cancelling MCP flexion torque. Restoring MCP extension torque, even with a weak or partially innervated muscle, would restore the capability of producing lateral force. Similarly, extensors are necessary to regulate MCP and IP torques to produce well directed palmar force. Thus, the limited regulation of flexion-

45

extension torques afforded by the transfer of even a weak muscle may impart the ability to direct

forces at the finger tip.

ii) Complementing tendon transfers with the adjustment of specific moment arms may improve force production outcomes

The magnitude of a given finger tip force is augmented by increasing the magnitude of the

torques at each joint while maintaining their relative proportions constant. If the available

musculature cannot increase one of the joint torques above a certain level (because of weakness in

original or transferred muscles), the appropriate moment arm can be increased to attain an

increased finger tip force with the available musculature.

For example, the "Zancolli lasso" (Zancolli, 1979) is an active tendon transfer used to prevent

or correct the "claw hand" deformity (i.e., hypertension of MCP and flexion of IP joints;

Figure III.1A) when intrinsic muscle function is lost (e.g., ulnar palsy). In the Zancolli lasso, the

FDS finger is transferred to wrap around the fibrous sheath of the MCP which also tugs on the

diagonal and lateral bands of the extensor mechanism (Figure III.1A), thereby restoring MCP

flexion and IP extension and preventing the clawing of the fingers. Unfortunately, the use of FDS

to exclusively flex the MCP reduces palmar force capabilities (compare Figure III.2B with

Figure III.2C). However, by surgically increasing the FDP moment arm (and correcting for the

increase in tendon excursion) at the PIP joint (Figure III.1C), the magnitude of palmar force can be

increased (cf. Figure III.2C with D). That is, proper positioning of the finger can be restored while

retaining adequate palmar force capability.

46
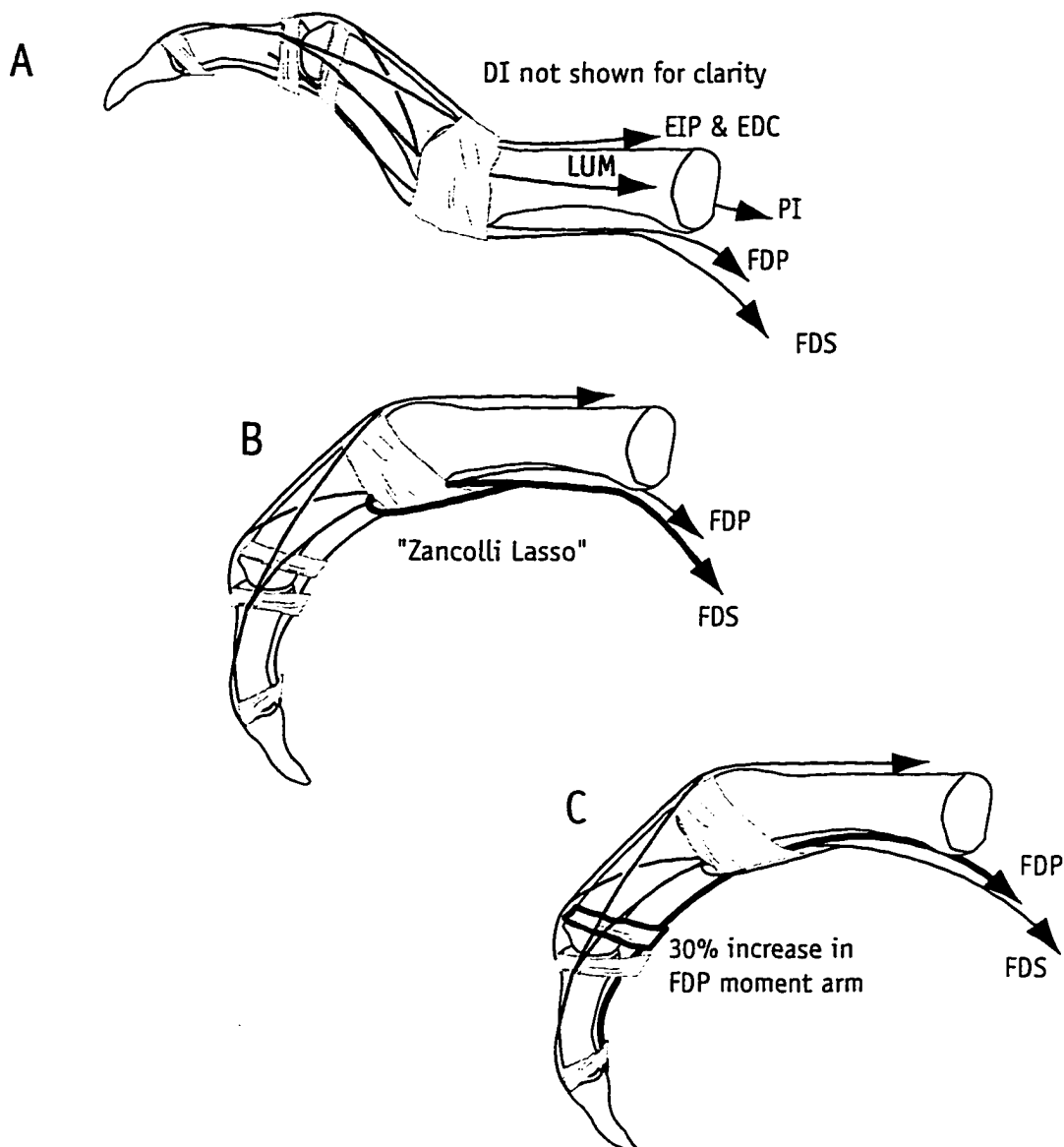
FIGURE III.1. Description of modified Zancolli lasso.
Schematic representations of the fibrous sheaths that function as tendon pulleys are included, DI muscle is not shown for clarity. (A) Claw deformity due to intrinsic muscle deficiency. (B) The Zancolli lasso restores intrinsic muscle function by using the FDP tendon to wrap around the fibrous sheath of the MCP which also tugs on the diagonal and lateral bands of the extensor mechanism. While indicated to correct the "claw deformity" it, however, reduces the force capabilities of the finger if the FDS to the same finger is used (Figure III.2C). (C) The force capabilities are improved by complementing the Zancolli lasso with a surgically enlarged FDP flexor moment arm at the PIP joint (Figure III.2D).

palmar force

palmar force

•••••• (A) Intact Model
—•— (B) Model without intrinsics
— — — (C) Zancolli Lasso
———— (D) Modified Zancolli Lasso

50 N
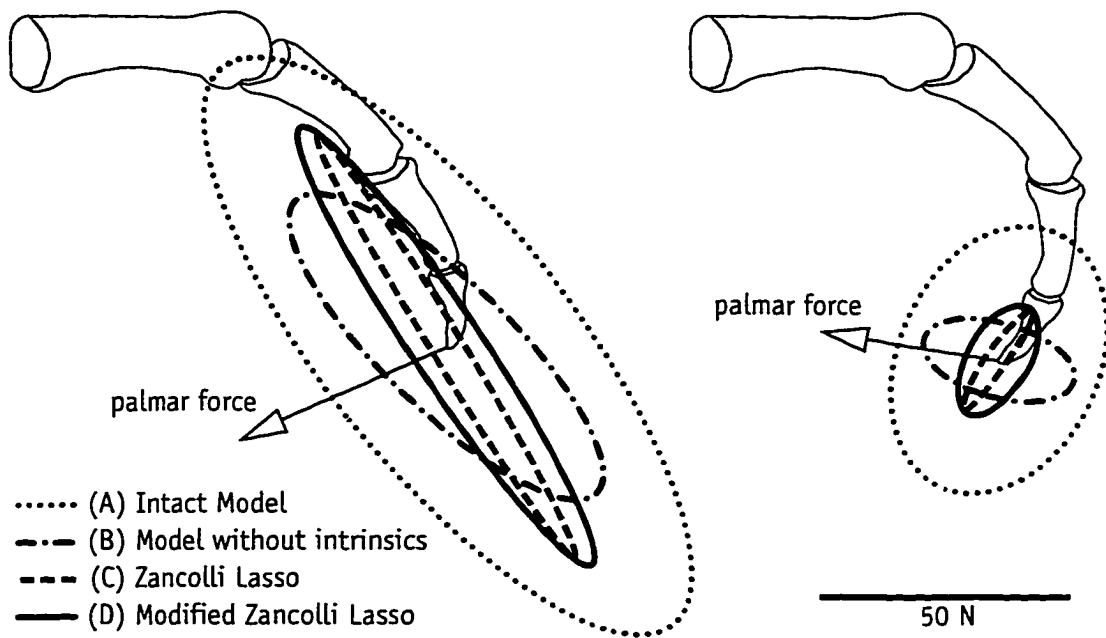
FIGURE III.2. Effect of modification of Zancolli Lasso on force production in plane of finger flexion. Point-force ellipsoids for the index-finger Model in Chapter I in two postures. (A) Intact finger. (B) After loss of intrinsic muscles. (C) After transfer of FDS to PI and LUM by the Zancolli lasso. Note the reduction in palmar force capability (Figure III.1B). (D) After modifying the Zancolli lasso by adding a 30% increase in the PIP moment arm of FDP (Figure III.1C).

IMPLICATION 2: THE LATERAL BANDS OF THE EXTENSOR MECHANISM ACT AS A FLOATING NET

The tendons of PI and LUM bifurcate to contribute to the proximal and terminal bands of the extensor mechanism (Figure III.1A). This geometric change induces a vectorial distribution of tension in which the algebraic sum of tensions in the tendon bifurcations is greater than the tension from which they originate (Figure III.3). This increases the magnitude of interphalangeal extensor torques without changes in moment arms or excitation level. This apportioning of tendon tension is predicted to affect the magnitude of distal force most (Table I.4 on page 23). Post-traumatic or post-operative adhesions in the extensor mechanism, which prevent the free gliding of the lateral bands, are expected to compromise the vectorial distribution of forces and may result in reduced distal force capabilities.
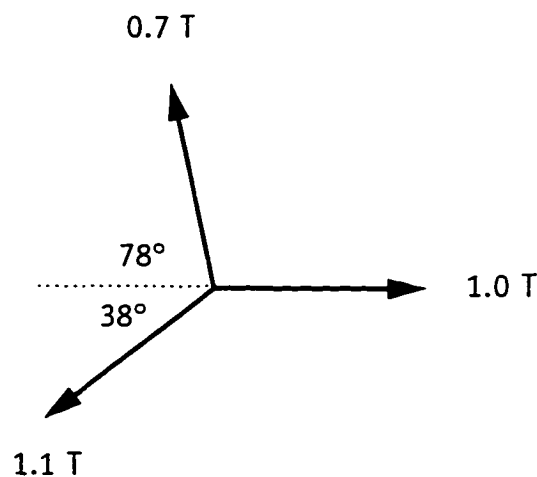
FIGURE III.3. Vectorial distribution of tension in a floating net. The tension magnitudes in each member achieve static equilibrium.

IMPLICATION 3: INDIRECT DETERMINATION OF MUSCLE OPTIMAL FIBER LENGTH

Knowing the region of the force-length (f-l) curve where donor muscles operate can only improve the design and execution of active tendon transfers. For a constant excitation under isometric conditions, a muscle will produce maximal force when its fibers are at a specific fiber length (i.e., the "optimal fiber length"), and active force output will decrease if the fibers are shortened or lengthened. Tendon excursions elicited by changes in finger and wrist posture affect muscle fiber length and, therefore, force production of individual muscles. Thus, when transferring a muscle, it is desirable to set its tendon length such that muscle fibers are close to optimum length when the finger is in the target posture. There exist accurate methods of estimating optimal fiber length (Lieber, *et al.*, 1994), but their intraoperative application is time consuming.

Biomechanical models alone cannot estimate optimum fiber length directly. The isometric force output of a muscle $f(e, l)$ is modeled by scaling maximal force of the muscle at optimum fiber length f_o, by excitation level e ($0 \leq e \leq 1$) and the position of its fibers in the force-length curve l ($0 \leq l \leq 1$) (the effect of fiber length changes can be represented by a scaling of maximal force with a value between zero and 1).

$$f(e, l) = \underbrace{\sigma \times PCSA}_{f_o} \times e \times l \qquad \text{EQ III.1}$$

where σ is the maximal muscle stress and **PCSA** the physiological cross sectional area of the muscle (Zajac, 1989). Because EQ III.1 is a multiplicative relationship, **PCSA**, e and l are redundant parameters. For example, increasing **PCSA** or excitation, or assuming the fibers to be closer to optimum length, all increase predicted muscle force.

Complementing biomechanical models with experimental measurements allows the indirect estimation of optimum fiber length. Whenever the force output of the finger is known at two or more postures for which a muscle is measured to be maximally excited, the location of that muscle in the force-length curve can be estimated. If the muscle is predicted to be maximally excited, any changes to PCSA necessary to predict the measured force at both postures indicates in which portion of the force length curve the muscle is acting.

For example, in Table I.6 on page 27, the PCSA of PI was reduced by 33% as the PIP joint extended. Because PIP extension shortens the fibers of the PI (PI is a PIP extensor), the apparent reduction in PCSA with fiber shortening suggests PI is acting in the ascending limb of the f-l curve. Similarly, MCP extension as the finger goes from intermediate to extended posture lengthens the PI fibers (PI is an MCP flexor). The apparent increase in PCSA with fiber lengthening also suggest that PI is in the ascending limb of the F-l curve. A similar analysis would suggest that DI is at the plateau of the f-l curve when the finger is in the intermediate and extended postures.

This method cannot be applied to the data collected from the extrinsic muscles in Chapter I because changes in fiber length due to finger posture changes were counteracted by changes in wrist posture in an effort to reduce the variability of EMG recordings. Thus, the predicted changes in PCSA in Chapter I may or may not be reliable indicators of fiber length changes.

APPENDIX A: FINE WIRE ELECTROMYOGRAPHIC RECORDING DURING FORCE GENERATION. APPLICATION TO INDEX FINGER KINESIOLOGIC STUDIES

By Charles G. Burgar, Francisco J. Valero-Cuevas, and Vincent R. Hentz

52

ABSTRACT

When accurately placed, fine wire electrodes (FWEs) permit selective electromyographic (EMG) recording during kinesiologic studies; however, their potential to limit contraction of the index finger muscles has not previously been established. Since these electrodes cannot be re-inserted, reliable techniques are necessary to achieve proper placement while minimizing subject discomfort and electrode waste. The small size, close arrangement, and anatomical variability of hand and forearm muscles create challenges to achieving these goals. In this study, we simultaneously measured maximal finger tip forces and selective EMG signals from all seven muscles of the index finger. Forces in five directions, with and without FWEs in place, were not statistically reduced in eight healthy subjects. To guide electrode placement, we identified skin penetration landmarks, direction of needle advancement, and depth of muscle fibers. Fibers of flexor digitorum superficialis and flexor digitorum profundus to the index finger were more distal than depicted in textbooks, requiring electrode placement at, or distal to the midpoint of the forearm. For these muscles and the extensor digitorum, locating the desired fibers first with a monopolar needle electrode facilitated subsequent FWE placement. For the dorsal and palmar interossei, lumbrical, and extensor indicis proprius, insertion was aided by concurrent monitoring of the EMG signals. We achieved a 93% success rate during FWE placement into a total of 60 muscles. Techniques for recording from each of the seven index finger muscles are described.

53

INTRODUCTION

Electromyographic (EMG) recordings using fine wire electrodes (FWEs) are often used for

selective recording of muscle activity in kinesiologic studies, including those of the index finger

(Boivin, *et al.*, 1969; Close and Kidd, 1969; Long, *et al.*, 1970; Law, *et al.*, 1989; Darling and Cole,

1990; Darling, *et al.*, 1994). Previous reports, however, have lacked sufficient detail to guide

electrode placement in all muscles of the index finger. The effect of indwelling FWEs on the

amplitude of maximal voluntary force production has not been established. Electrode insertion

methods described in clinical EMG texts (Goodgold, 1984; Chu-Andrews, 1986; Perotto, 1994) are

not intended for selective recording from extrinsic muscle fibers to specific fingers. The usual

approach to lumbrical and palmar interosseous muscles is through the sensitive skin of the palm,

which may interfere with hand function during recording and is particularly uncomfortable

during insertion. Kinesiologic studies of the index finger muscles using FWEs present special

challenges. Positioning the electrodes in specific fibers is often difficult because the muscles may

be small in diameter, located near fibers of other muscles or adjacent to neurovascular structures,

and may have variable anatomy (Brand and Hollister, 1993; Cole, 1995; Williams, 1995). Deep

muscles can not be palpated and must be located using surface landmarks. Selective recording

from certain bellies to the index finger is especially difficult with current electrode insertion

techniques. Some investigators use a "guided" technique during fine wire insertion (Park and

Harris, 1996); however, if the wires do not pass though the desired region during initial insertion,

it is not possible to withdraw and reposition this type of electrode. An improperly placed FWE

must be removed and another attempt made with a new electrode. Rigid needle electrodes

(monopolar or concentric) can be repositioned until within the desired fibers but movement of the

recording surface within the muscle during functional tasks may explain the within-study

variability previously reported (Maier and Hepp-Reymond, 1995b; Maier and Hepp-Reymond,

1995a). The discomfort produced by muscle contraction with rigid needles in place may prevent

maximal effort. FWEs are anchored within the muscle and usually move with it. In our ongoing

studies of maximum index finger force generation (Chapters I-III; (Valero-Cuevas, *et al.*, 1996)), we

modeled finger force production based on muscle activation levels. Our initial attempts to place

FWEs using standard clinical EMG landmarks (Goodgold, 1984; Chu-Andrews, 1986; Perotto,

1994) often failed to achieve adequate selectivity for fibers that exclusively flex or extend the index

finger. Even with EMG monitoring during advancement of the inserting needle, as described by

Park and Harris, satisfactory recordings were rarely achieved without multiple trials, each

producing discomfort for the subject and requiring a new FWE. To improve placement accuracy,

we carried out dissections of four upper extremities from three cadavers. In the first specimen, we

injected dye using clinical EMG landmarks and identified the stained tissue. For the majority of

sites, placement using surface landmarks yielded unacceptable accuracy. The anatomy of the

muscles of interest, fiber orientation, and relationships to surrounding structures were

investigated with the assistance of an experienced hand surgeon (VRH). We found the location of

the extrinsic index finger flexor muscle fibers to be more distal than depicted in EMG reference

publications. The digastric conformation of the flexor digitorum superficialis to the index finger, as

described previously (Close and Kidd, 1969; Agee, *et al.*, 1991; Brand and Hollister, 1993), was

confirmed. We also identified dorsal approaches to selected intrinsic hand muscles. Considering

the results of the dissections, we devised techniques to record from all seven muscles of the index

finger using FWEs without piercing the palm of the hand and without discernible cross talk. For

some muscles, we found it helpful to first use a monopolar needle electrode (MNE) to identify the

location of the desired fibers, then followed a similar trajectory while replacing the MNE with a

FWE. We validated our electrode placement techniques in ten subjects. In five of these subjects, we

measured the effect of indwelling FWEs by measuring maximal voluntary force production before

and after placement. We present these results as an aid to others studying hand biomechanics, as well as for clinicians and investigators performing precise needle placement within index finger and other skeletal muscles.

MATERIALS AND METHODS

Subjects

Ten healthy subjects (six females, four males) without evidence of neurologic or orthopedic impairment of the upper limbs participated in this study. The mean age was 27 ±6 (SD) years. All subjects demonstrated normal isolated control of upper limb muscles, including the ability to produce graded contractions. This study was approved by the Medical Committee for Protection of Human Subjects in Research at Stanford University and each subject gave written informed consent prior to participation.

Instrumentation

We fabricated FWEs using a technique adapted from published techniques (Basmajian and De Luca, 1985; Loeb and Gans, 1986). The insulation at one end of wires 50 microns in diameter and 150 mm in length (P/N 431, stainless steel alloy, 0.002 in diameter, nylon insulation, Driver-Harris Co. Harrison NJ) was removed by passing it quickly through a butane flame. Residue was removed with an alcohol pad. Each wire was trimmed so that 2 mm of conducting surface was exposed. The untrimmed ends of two wires were threaded through the bevel of a stainless steel hypodermic needle (25 mm, 27 gauge or 37 mm, 25 gauge). Folding the trimmed ends of the wires (6 mm of one wire and 3 mm of the other) back along the side of the needle formed barbs with exposed surfaces that did not overlap. We sterilized the electrodes by exposure to ethylene oxide.

Whenever satisfactory placement was likely to require electrode repositioning, we first used disposable monopolar EMG needle electrodes (P/N 902-DMG37, TECA Corporation, Pleasantville, NY), referenced to a 30 mm surface electrode, to locate the desired fibers. Redux® Creme (Hewlett-Packard Medical Products Group, Waltham, MA) served as the electrolyte for reference and ground electrodes. An 8-channel electromyograph (Viking IIe, Nicolet Instrument Corporation, Madison, WI) amplified, filtered, displayed, and provided auditory output of the EMG signals. We visually monitored the raw EMG signals for artifact. A filter bandpass of 100 Hz-20 kHz, typical, minimized 60 Hz interference, rejected movement artifact, and enhanced selectivity. Full-wave rectification and smoothing (20 ms time constant) using custom analog circuits produced the envelope of the EMG signal. An Apple Macintosh Quadra 950 computer with a multifunction input/output board and data acquisition software (NB-MIO-16 and LabVIEW, National Instruments, Austin, TX) sampled and stored the EMG signal envelope at 200 samples per second. We measured fingertip forces against the low-friction surface of a 3-axis transducer (130 N maximum, 0.1 N resolution, F/T Gamma, Assurance Technologies, Garner, NC) that was mounted on the end of a robotic arm (Puma™ 260, Stäubli-Unimation, Inc. Duncan, SC). The robot was pre-programmed to rapidly and accurately position the force transducer to measure force in five directions. To prevent generation of significant shear forces between the finger tip and the transducer, custom-fit plastic thimbles with 5 mm ball bearings imbedded into the outer contact surfaces were worn on the end of the index finger.

Experimental Design

Subjects were asked to generate a complete series of finger force measurements without EMG monitoring, and then again the following day while EMG activity was recorded. The finger was maintained in neutral ad-abduction, 45° flexion at metacarpophalangeal and proximal

interphalangeal joints, and 10° flexion at distal interphalangeal joint; wrist in 80° extension and neutral radial deviation; index not resting against middle finger. Video monitoring ensured replication of finger and hand test postures. Under each test condition, subjects were instructed to generate the maximum possible force between the tip of the index finger and the surface of the transducer. Additional details of the testing apparatus and finger postures have been described in Chapters I-III.

Electrode Placement

Skin penetration occurred under aseptic conditions. During electrode placement and verification of signal quality, subjects lay supine on an examining table. They were instructed to report unexpected pain or sensations. Local anesthetic agents were not used. No adverse effects, other than occasional mild local discomfort lasting up to two days, were reported. Following electrode insertion into muscles of the right upper extremity, subjects moved to the force measurement workstation where they sat in a chair with their forearm resting in a trough and their right hand gripping a vertical dowel. In two subjects, we validated our method of electrode placement only in the extrinsic flexor muscles of the index finger. In the remaining eight subjects, we targeted all seven muscles of the same digit. Electrodes typically remained in place for 1.5-2 hours. At the beginning and end of each session, we tested each EMG channel to verify its response and selectivity. The surface landmarks, needle trajectory, and methods for confirming accurate and selective EMG recording are described for each of these muscles.

Electrical stimulation through the fine wire electrode was not considered a reliable estimate of electrode location because false positives can be obtained when i) the electrode is outside the target fibers, but close enough to their terminal motor nerves or ii) the electrode is inside undesired fibers

and the large pulse current or duration necessary to stimulate muscle fibers directly is sufficient to

stimulate the terminal motor nerves of the target fibers.

Flexor digitorum superficialis (FDS) fibers to index finger

Anatomy

The FDS originates in the proximal forearm as two heads. A humeroulnar head arises from the

common flexor tendon from the medial epicondyle of the humerus, from deep antebrachial fascia,

from the ulnar collateral ligament of the elbow joint, and from the medial side of the coronoid

process of the ulna. A radial head arises from the proximal two-thirds of the anterior border of the

radius. The FDS is partially covered by the flexor carpi ulnaris, palmaris longus, and flexor carpi

radialis. Fibers of the FDS form two planes. Those arising from the radius lie in a superficial plane

to connect with the tendon to the middle finger. The tendon to the ring finger originates from

fibers in the superficial plane that arise from the common flexor tendon, as well as from fibers

arising from an intermediate tendon. Brand recently described a fusiform muscle belly arising

proximally from the common flexor tendon and inserting on an intermediate tendon that, in turn,

serves as the origin for muscle bellies to the ring, little, and index fingers (Brand and Hollister,

1993). The muscle fibers and tendons to the latter two fingers lie in the deeper plane of the FDS and

may be found in the distal half of the forearm. The FDS tendons insert on the volar surfaces at the

bases of the middle phalanges and have the capacity to perform flexion of the

metacarpophalangeal joint (MCP) and proximal interphalangeal (PIP) joints of the second through

fifth digits, as well as the wrist. Important variations in the origin and interconnections of the

individual muscle bellies, however, have been reported (Close and Kidd, 1969; Agee, *et al.*, 1991).

Electrode Placement Technique

We identified the tendons of the superficial flexor group in the distal half of the forearm and measured the distance between the elbow crease and the distal wrist crease (De-w). We first inserted a monopolar electrode percutaneously over the lateral (radial) border of the ulna, just medial to the flexor carpi radialis (FCR) tendon, and proximal to the distal wrist crease by 30% of De-w (Figure A.1). The electrode was angled toward the medial border of the radius and advanced while monitoring the audio produced by EMG activity. Slight, rapid flexion and extension of all digits, alternating with similar movement by only the index finger, provided a "homing signal" to guide electrode placement and helped detect contact with tendons and, thus, avoid their penetration. We repositioned the electrode tip, as necessary, to produce crisp, loud bursts of EMG activity synchronous with index finger PIP joint flexion. The depth of penetration was typically 10-20 mm. After comparing their relative lengths, we inserted a FWE parallel to the MNE and advanced it until the bare recording surfaces of the wires were at approximately the same depth as the tip of the monopolar electrode. Once a satisfactory signal was obtained from the FWE, we removed the MNE and the hypodermic FWE insertion needle, leaving only the wires in place.

Test Maneuvers

We considered the placement satisfactory when strong resisted flexion of the index finger PIP joint produced a full interference pattern (oscilloscope baseline obscured by motor unit action potentials) but resisted flexion of all other joints of the hand produced no discernible potentials.

Pitfalls

Whenever tingling or an electrical sensation in the hand was reported, the electrode should be slightly withdrawn and re-oriented before further advancement to avoid piercing the median nerve. If inserted medial to the FDS, the electrode will enter the slip to the little finger. If too deep,

the electrode will enter the flexor profundus or pronator quadratus. Too lateral a placement targets

the flexor pollicis longus.

Flexor digitorum profundus (FDP) fibers to the index finger

Anatomy

The superficial layer of forearm flexor muscles and the FDS cover the FDP. It has a broad

origin from the proximal three-fourths of the ulna, from the interosseous membrane, and from the

deep antebrachial fascia. Like the FDS, the FDP ends in four tendons, one to each finger. The fibers

to the index finger often form a separate belly throughout most of the forearm while formation of

the other finger tendons occurs at more variable levels. The FDP tendons lie in a single plane deep

to the tendons of the FDS at the wrist, insert onto the anterior surfaces at the base of the distal

phalanges and flex all joints of the fingers. The FDP may also assist with wrist flexion.

Electrode Placement Technique

We entered the fibers of FDP in a manner similar to that described for placement within FDS.

We inserted a monopolar electrode over the medial border of the radius at one-half De-w

(Figure A.1). While monitoring the EMG audio, the electrode was advanced perpendicular to the

skin or angled slightly toward the ulna, passing through the FCR to a depth of approximately 30

mm. The index finger was held in light resisted flexion at the distal interphalangeal joint and the

electrode repositioned until located within active fibers. After satisfactory positioning, the

monopolar electrode served as a guide for inserting a FWE, and was then removed.

61

Test Maneuvers

We verified adequate placement by observing EMG responses during sequential flexion of each joint of the thumb and fingers, while stabilizing all other joints in extension.

Pitfalls

When placing electrodes in large forearms, we found it necessary to use 50 mm monopolar and hypodermic insertion needles to reach the FDP. The median nerve typically lies between the FDS and FDP in the mid-forearm and care should be taken to avoid its penetration. The flexor pollicis longus, radial artery, and superficial radial nerve lie lateral to the insertion site. The interosseous membrane, nerve, and artery lie deep to FDP. If too superficial, the electrodes will be in the FCR or FDS. If too medial, it will enter the FDP belly to the middle finger.

Extensor indicis proprius (EIP)

Anatomy

This muscle originates from the posterior surface of the ulna and from the interosseous membrane, distal to the origin of the extensor pollicis longus. The muscle fibers and tendon angle radially and distally to insert into the extensor expansion of the index finger, along with the extensor digitorum communis (EDC) tendon. Contraction of the EIP results in extension of the index finger at all joints, and assists in adduction of this digit.

Insertion Technique

The anatomy of the EIP permits FWE placement without the need for fiber localization with a monopolar electrode. Our approach followed common clinical EMG guidelines.[9] We inserted a FWE needle between the ulna and the tendons of the finger extensor muscles, 40-50 mm proximal

to the ulnar styloid (Figure A.2). The EMG audio was monitored and the index finger maintained in extension against minimal force while the electrode was advanced into actively firing motor fibers. The recording contacts were typically 5-15 mm beneath the skin surface.

Test Maneuvers

A full interference pattern during resisted index finger extension and electrical silence during resisted extension of the thumb and other fingers indicated successful placement.

Pitfalls

Placement within the muscle fibers of the extensor pollicis longus or extensor pollicis brevis can occur if the insertion is too proximal or radial. Care should be taken not to penetrate the extensor carpi ulnaris or extensor digiti minimi tendons, which lie medial and lateral to the typical insertion trajectory. Alternating flexion and extension of the little finger should not cause movement of the hypodermic needle.

Extensor digitorum (EDC) fibers to index finger

Anatomy

The EDC originates from the common extensor tendon at the lateral epicondyle of the humerus. It inserts, after dividing into four tendons, onto the dorsum of the middle and distal phalanges of the fingers. The tendon to the index finger joins with that of the EIP to insert into the extensor expansion. The EDC extends the MCP joints and, in combination with the interossei and lumbricales, extends the interphalangeal joints. It also assists in abduction of the index, ring, and little fingers.

Insertion Technique

Although the EDC is superficial and can often be easily palpated, we employed a MNE for localization because of the frequent presence of EMG signals from fibers of EDC to the middle finger. We inserted the electrode perpendicular to the skin, along the line connecting the lateral epicondyle and the knuckle of the index finger, at one-third of the distance of this line (Figure A.2). The electrode was advanced to a depth of 10-30 mm while monitoring for activity caused by slight extension of the index finger. If activity was present upon extension of the wrist or other fingers, the electrode was withdrawn and redirected. If activity isolated to index finger extension was not found, the electrode was removed and re-inserted 10-20 mm distally. If tendon was encountered, the electrode was repositioned proximally. When the MNE recording was satisfactory, we replaced it with a FWE.

Test Maneuvers

Placement was successful when a full interference pattern was obtained during resisted index finger MCP extension with electrical silence during resisted extension of the other fingers and of the wrist.

Pitfalls

During wrist extension to test for cross-talk from extensor carpi radialis, simultaneous flexion of the index finger MCP joint was often necessary to minimize contraction of EDC. We employed a similar technique, using simultaneous flexion of index finger MCP and extension of middle finger MCP joints, when testing for absence of EMG activity from middle finger fibers.

First dorsal interosseous (DI)

Anatomy

Fibers of DI arise from the medial border along the proximal half of the first metacarpal and from the lateral surface of the second metacarpal. They insert into the base of the proximal phalanx of the index finger. Insertion into the extensor expansion may occur, but is not common (N.B.: seen in 25% of Japanese population; (Ikebuchi, *et al.*, 1988)). This muscle acts to abduct the index away from the middle finger, assists in flexion of the MCP joint, and may also adduct the thumb.

Insertion Technique

We placed FWEs into DI following the common clinical EMG approach and without first using a monopolar electrode. We passed the FWE through the dorsum of the hand, just radial to the midpoint of the second metacarpal bone (Figure A.3). The index finger was abducted against minimal resistance, EMG audio monitored, and the wire tips advanced to a typical depth of 5-10 mm.

Test Maneuvers

A full interference pattern during resisted index finger abduction and electrical silence during slight simultaneous adduction of the thumb and index finger indicated a successful placement.

Pitfalls

Too lateral an approach results in placement of the FWE in the adductor pollicis.

65

First palmar interosseous (PI)

Anatomy

The PI originates along the length of the ulnar surface of the second metacarpal bone and inserts into the extensor expansion and base of the proximal phalanx of the index finger on the ulnar side. In addition to adduction of the index toward the middle finger, the PI assists in MCP flexion with IP joint extension.

Insertion Technique

We inserted a FWE through the dorsal hand surface between the knuckles of the second and third digits, in a proximal and radial direction, toward the ulnar border of the second metacarpal bone (Figure A.3). The needle was angled 30-45° to the skin surface. A mild resistance to adduction of the index toward the middle finger was maintained and the electrode advanced until the EMG signal indicated that the electrode was positioned within fibers of PI.

Test Maneuvers

To insure freedom from crosstalk from lumbrical and dorsal interosseous muscles, the EMG activity during adduction was compared to signals generated during weak index finger MCP joint flexion with IP extension and during radial movement of the middle finger toward the thumb.

Pitfalls

If placed superficially, the FWE may record from the second dorsal interosseous muscle. If the FWE is angled in an ulnar direction, the second palmar interiors may be entered.

66

First lumbrical (LUM)

Anatomy

The LUM arises from the distal tendon of the FDP and inserts into the extensor expansion of the index finger. Contraction of LUM flexes the MCP and extends the IP joints of the index finger.

Insertion Technique

We avoided penetration of the glabrous (hair-free) skin of the palm because electrodes inserted through this surface can interfere with grip and cause unnecessary pain. Instead, we employed a subcutaneous approach from the first web space (Figure A.3). Palpation of the belly of LUM during resisted forceful 90° MCP joint flexion, while maintaining IP joint extension, permitted a target location to be identified where this muscle crosses the transverse palmar crease (slightly radial to the flexor tendons). The needle was inserted 5-10 mm proximal to the radial end of the same palmar crease, parallel to the skin surface, until within the fibers of the LUM.

Test Maneuvers

Recruitment of EMG activity during MCP flexion and silence during isolated index finger abduction and thumb adduction confirmed proper positioning.

Pitfalls

Palmar distraction of the skin of the web space helped avoid DI penetration.
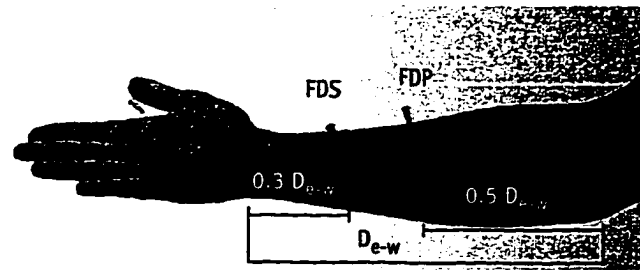
Figure A.1
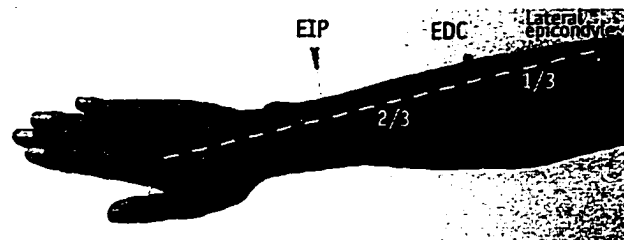
Figure A.2
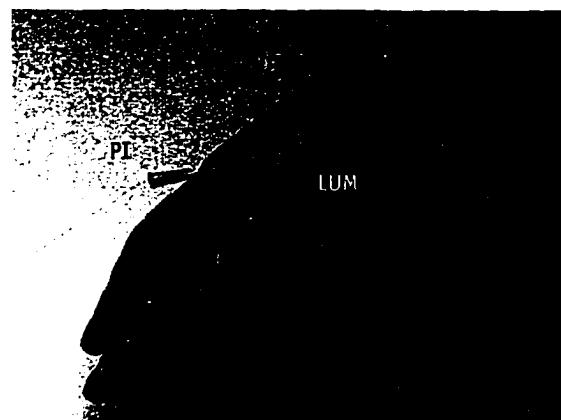
Figure A.3
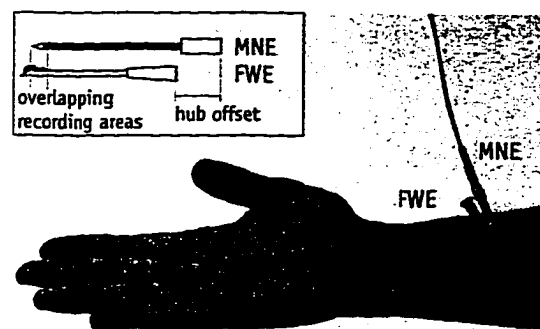
Figure A.4

FIGURE A.1. Fine wire electrode insertion in to FDS and FDP.

FIGURE A.2. Fine wire electrode insertion into EIP and EDC.

FIGURE A.3. Fine wire electrode insertion into the index finger intrinsic muscles.

FIGURE A.4. The MNE serves as a guide for subsequent FWE placement.

Comparing the lengths of the needle shafts and their respective recording surface locations prior to use (insert) facilitates placement within the same muscle fiber territory.

RESULTS

Selective EMG Recording

We attempted to record from all seven muscles of the index finger in each of eight subjects,

and from the FDS and FDP in two additional subjects (60 muscles, total). Fine wire EMG recording

of activity isolated to the intended muscle fibers was achieved for 93% of the target sites.

Figure A.5 demonstrates the typical levels of crosstalk and artifact observed.
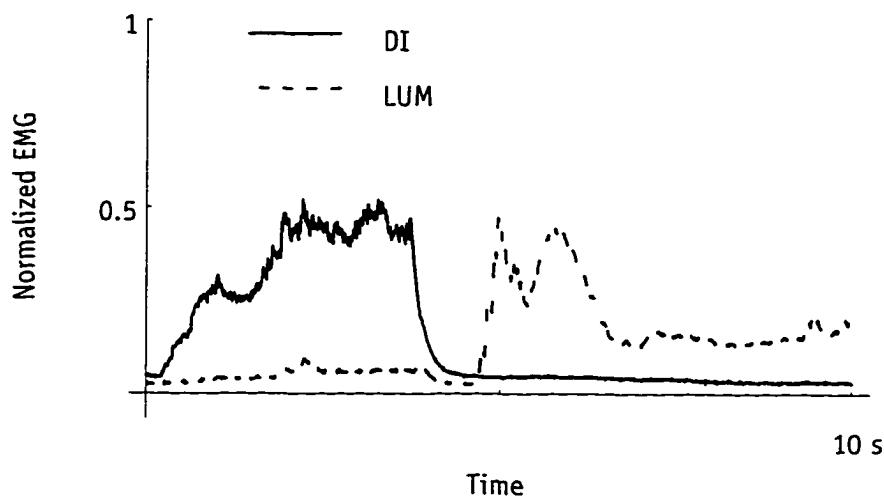
FIGURE A.5. Crosstalk levels in EMG recordings.
Simultaneous recordings showing typical crosstalk between DI and LUM during
sequential resisted radial abduction, followed by isolated flexion of the MCP.
The index finger remains extended at the interphalangeal joints.

Reliable data was unobtainable from four sites. The desired signal could not be obtained

without significant crosstalk in one FDP and one FDS, apparently due to adjacent fibers to the

middle finger. One electrode was removed in mid-experiment from the PI due to pain and reduced

signal amplitude. The electrode intended for the PI recorded activity primarily from the second

dorsal interosseous in one subject. The signal from a fifth electrode, for the FDS, was usable but

crosstalk from the middle finger fibers of FDS could not be completely eliminated. We occasionally

69

experienced a loss of signal while advancing the FWE, probably due to contact between the bare

wire tips and the metal needle. Slight rotation of the needle shaft usually restored the signal.

Effect of Indwelling FWEs on Force Production

The results of repeated force measurements, with and without the FWEs in place, are shown in

Figure A.6. According to repeated measures analysis of variance, the presence of FWEs during

force measurements did not significantly alter index finger force magnitudes ($p < 0.46$).
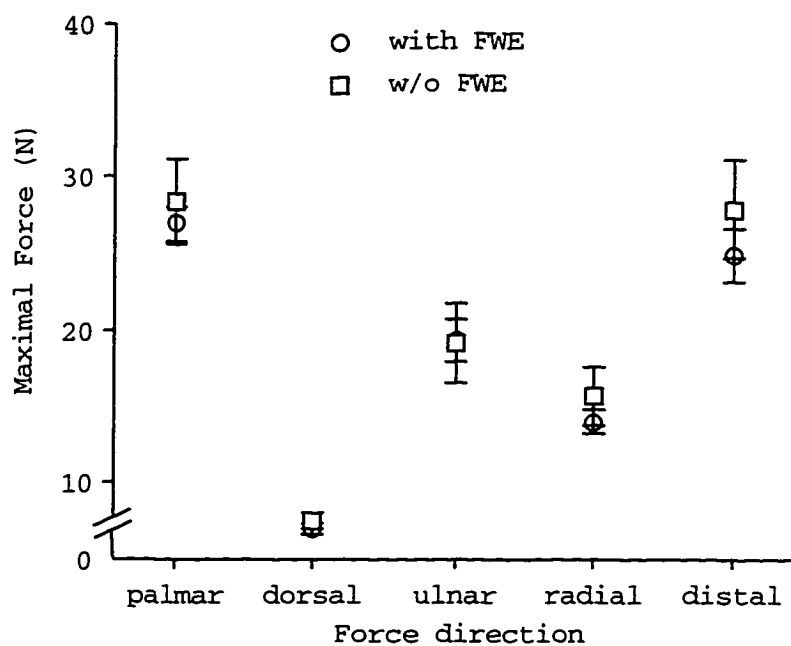
FIGURE A.6. Adjusted mean ($\pm$SE) of finger force magnitudes with and without FWE.
Maximal static finger forces produced in three standardized finger postures showed no statistically significant change with the presence of fine wire electrodes ($p < 0.46$). Note that the adjusted mean has already corrected for posture and subject differences. Forces emanate from the midpoint of the distal phalanx, and perpendicular to it, in the palmar, dorsal, ulnar and radial directions. Distal force emanates from the finger tip, parallel to the distal phalanx (see Chapter I)

DISCUSSION

Placement of the FWEs and contraction of muscles during force measurement were generally well tolerated. Only one electrode caused discomfort that became intolerable. The reduction of signal amplitude accompanying the pain was believed to indicate local intramuscular bleeding, so that electrode was removed. Although it was typically necessary to reposition the needle into several locations while seeking an acceptable signal, initial fiber localization with a MNE was tolerated without complaint and was preferred over multiple FWE insertions. For the FDS, FDP, and EDC, initial use of a MNE allowed the EMG signal to be sampled and, if necessary, for the electrode to be withdrawn and re-directed into another area. This technique may be employed any time the success of a single FWE insertion is uncertain. If placement is suboptimal, FWEs can only be advanced farther (assuming the hypodermic needle is still in place); withdrawal of the needle used to place FWEs leaves the wire tips imbedded in the tissue. With the use of aseptic technique, it is common clinical practice to use one disposable MNE for multiple insertions in an individual patient. A concentric needle electrode could also be used to locate target areas. It was helpful to compare the configuration of the fine wire and monopolar needles before insertion so the recording surfaces of the electrodes could be placed at an equal depth (Figure A.4).

The difficulty encountered in FDS recording can be accounted for by the anatomical and functional complexity of this muscle. The ability to independently flex the PIP joint of each finger stems from the subdivision of FDS into slips controlling each finger. However, a proximal, common belly contributes to flexion of the index, ring, and, frequently, the little fingers through an intermediate tendon, as described above. Activity recorded by electrodes inserted into the common belly may not be specific for flexion of a single digit. We found the distal bellies of FDS to be quite thin in some cadavers. Successful placement of both electrode wire tips within one belly would depend, in such cases, on the angle at which the needle enters the muscle. The method used

71

to record from the FDS in this study differs from previous approaches and resulted in a high success rate. The digastric configuration of this portion of the muscle and the anatomical variability present a challenge to electrode placement. We compensated for these factors by inserting the FWE more distally (in the belly directly attached to the index finger tendon) and by conducting a search for the target fibers with a MNE prior to FWE placement. For the FDP, electrode insertion from the ulnar aspect of the forearm requires a longer needle to reach the fibers to the index finger than a volar approach. Medial insertion is also more likely to result in the placement within portions of the muscle that flex other fingers. In our subjects, the fibers attaching to the index finger were segregated in the mid-forearm, allowing selective recording from FDP. Attempts at more proximal placements usually yielded significant activity with flexion of other digits. Listening to the raw EMG audio during electrode insertion provided continuous guidance and an indication of adequate placement. Electrical stimulation through the electrode while observing the mechanical response may offer certain advantages (Geenen, *et al.*, 1996); however, we find it less useful for predicting EMG crosstalk in the recorded signal. To obtain the advantages of both methods, a switch may be used to rapidly alternate between stimulating and recording through the electrode (Burgar and Valero-Cuevas, 1996). The ability to detect activation of functional groups of muscle fibers may be a useful tool for improving models of musculoskeletal force generation and neuromuscular coordination. Enhanced recording accuracy may also facilitate clinical assessment of gait impairment and movement disorders

CONCLUSIONS

This study demonstrates the feasibility of simultaneously measuring finger tip force

generation and EMG activity without significant influence from indwelling FWEs in all seven

muscles of the index finger. The FWE placement methods described in this article provided a high

level of accuracy and reliability. The use of EMG audio monitoring and initial fiber location with a

semi-rigid electrode may be applicable to EMG recording from other muscles, as well.

73

APPENDIX B: ADDITIONAL DATA

NB: In six subjects, we also recorded finger forces in the palmar direction without using a ball bearing. The smooth, flat surface of the thimble made direct contact with the force sensing surface, allowing the production of finger output torque (which we could not measure), resulting in a non-point force in the palmar direction which we call "paltor." While the force was directed with an accuracy similar to the other fore directions, there were no significant EMG groupings for this force. This suggests that subjects produced different levels of finger output torque which increased the variance in EMG, or that not enough samples were taken to detect a statistical difference in EMG levels.

NORMALIZED EMG LEVELS

The groups were obtained with ANOVA post-hoc pairwise comparisons (p< 0.05).

Dorsal Force | Palmar Force

Flexed

	Count	Mean			
fp	21	.27	a		
fs	21	.31	a		
di	24	.31	a		
lum	24	.41	a	b	
pi	18	.47		b	
ec	24	.59			c
ei	24	.76				d

Flexed

	Count	Mean		
pi	18	.11	a	
di	25	.29		b
fs	21	.30		b
lum	25	.32		b
ei	25	.33		b
ec	25	.37		b
fp	21	.41		b

Intermediate

	Count	Mean			
di	24	.18	a		
fp	21	.18	a		
fs	21	.24	a		
pi	18	.29	a	b	
lum	24	.40		b	
ec	24	.67			c
ei	24	.76			c

Intermediate

	Count	Mean			
ei	23	.17	a		
pi	17	.19	a		
fs	20	.26	a		
ec	23	.29	a	b	
lum	23	.29	a	b	
fp	20	.43		b	c
di	23	.45			c

Extended

	Count	Mean			
di	25	.15	a		
fp	22	.18	a		
fs	22	.20	a		
pi	19	.23	a		
lum	25	.46		b	
ec	25	.66			c
ei	25	.69			c

Extended

	Count	Mean				
ei	25	.09	a			
pi	18	.28		b		
ec	25	.32		b		
fs	22	.37		b	c	
lum	25	.48			c	d
fp	22	.53				d
di	25	.60				d

TABLE B.1. Normalized EMG levels for dorsal and palmar forces at all postures

Paltor Force

Distal Force

Flexed

	Count	Mean			
pi	15	.10	a		
ec	18	.20	a	b	
ei	18	.20	a	b	
di	18	.32		b	c
lum	18	.33		b	c
fs	15	.38		b	c
fp	15	.46			c

Flexed

	Count	Mean			
ei	23	.07	a		
ec	23	.10	a		
fs	20	.38		b	
fp	20	.43		b	
lum	23	.45		b	
di	23	.58			c
pi	17	.64			c

Intermediate

	Count	Mean			
pi	15	.10	a		
ec	18	.20	a	b	
ei	18	.20	a	b	
di	18	.32		b	c
lum	18	.33		b	c
fs	15	.38		b	c
fp	15	.46			c

Intermediate

	Count	Mean				
ec	25	.16	a			
ei	26	.22	a			
fp	23	.35		b		
fs	22	.45		b	c	
lum	26	.47		b	c	
di	26	.56			c	
pi	19	.72				d

Extended

	Count	Mean			
di	25	.15	a		
fp	22	.18	a		
fs	22	.20	a		
pi	19	.23	a		
lum	25	.46		b	
ec	25	.66			c
ei	25	.69			c

Extended

	Count	Mean			
ei	26	.16	a		
fs	23	.23	a		
ec	26	.25	a		
fp	23	.26	a		
di	26	.40		b	
lum	26	.45		b	
pi	19	.56			c

TABLE B.2. Normalized EMG levels for paltor and distal forces at all postures

Lateral Force

Flexed

	Count	Mean				
fs	22	.13	a			
fp	22	.20	a	b		
lum	25	.22	a	b		
di	25	.29		b	c	
pi	19	.37			c	d
ei	25	.41			c	d
ec	25	.45				d

Intermediate

	Count	Mean		
fp	22	.16	a	
pi	19	.26	a	
lum	25	.28	a	
fs	22	.30	a	
ec	25	.47		b
di	25	.52		b
ei	25	.60		b

Extended

	Count	Mean					
pi	17	.13	a				
fp	20	.14	a				
fs	20	.29		b			
lum	23	.39			c		
ei	23	.55				d	
ec	23	.58				d	e
di	23	.66					e

Medial Force

Flexed

	Count	Mean		
pi	18	.25	a	
ec	24	.26	a	
ei	24	.28	a	b
fp	21	.32	a	b
fs	21	.33	a	b
lum	24	.35	a	b
di	24	.43		b

Intermediate

	Count	Mean		
ec	24	.17	a	
di	24	.21	a	
lum	24	.22	a	
fp	21	.22	a	
fs	21	.24	a	
pi	18	.35		b
ei	24	.41		b

Extended

	Count	Mean					
di	24	.07	a				
lum	24	.17	a	b			
ec	24	.23		b	c		
fp	21	.28		b	c		
fs	21	.34			c	d	
ei	24	.42				d	e
pi	18	.48					e

TABLE B.3. Normalized EMG levels for lateral and medial forces at all postures

COMPARISON OF EMG TO MODEL-GENERATED
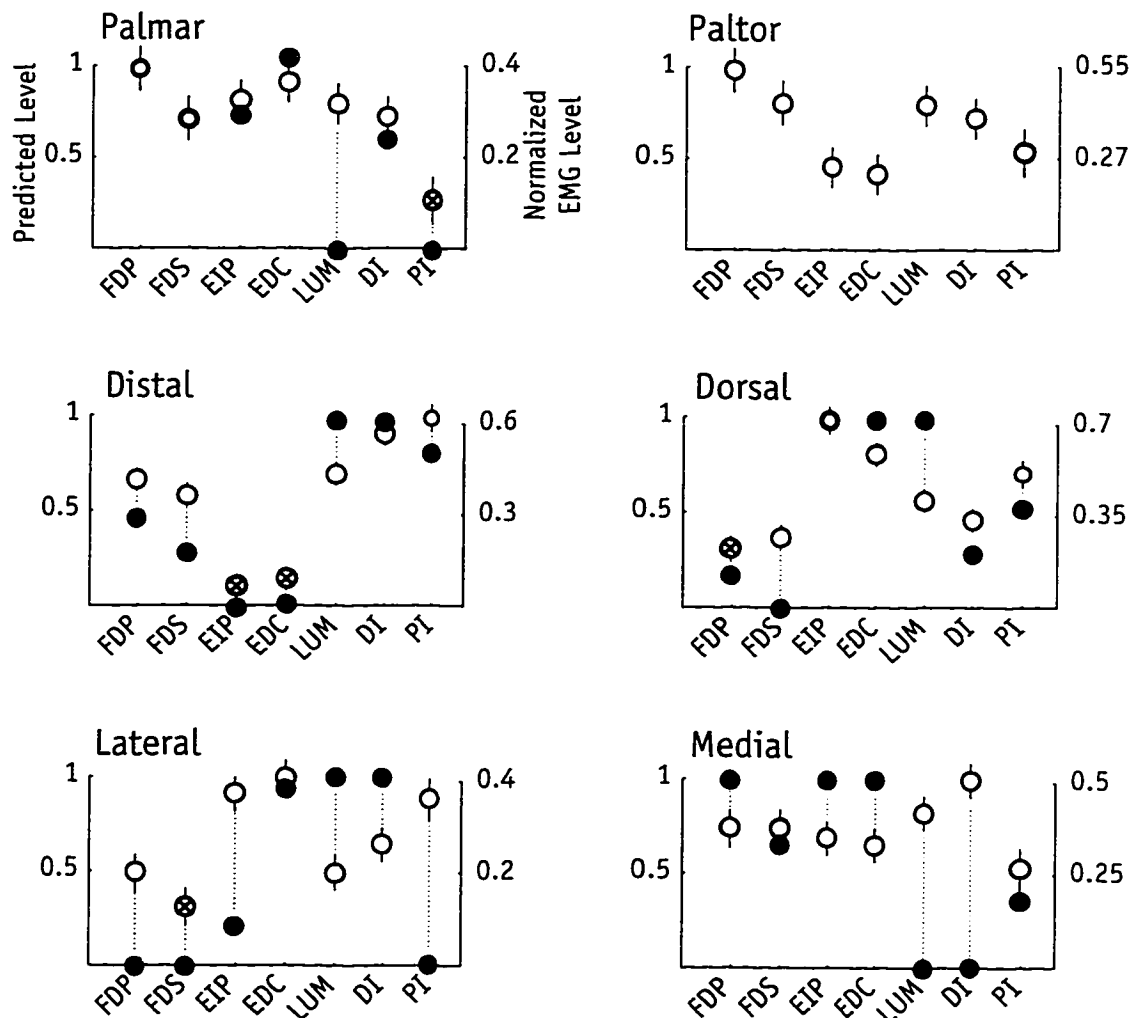
EXCITATIONS

FIGURE B.1. Comparison of EMG to model-generated excitation for **flexed posture.**
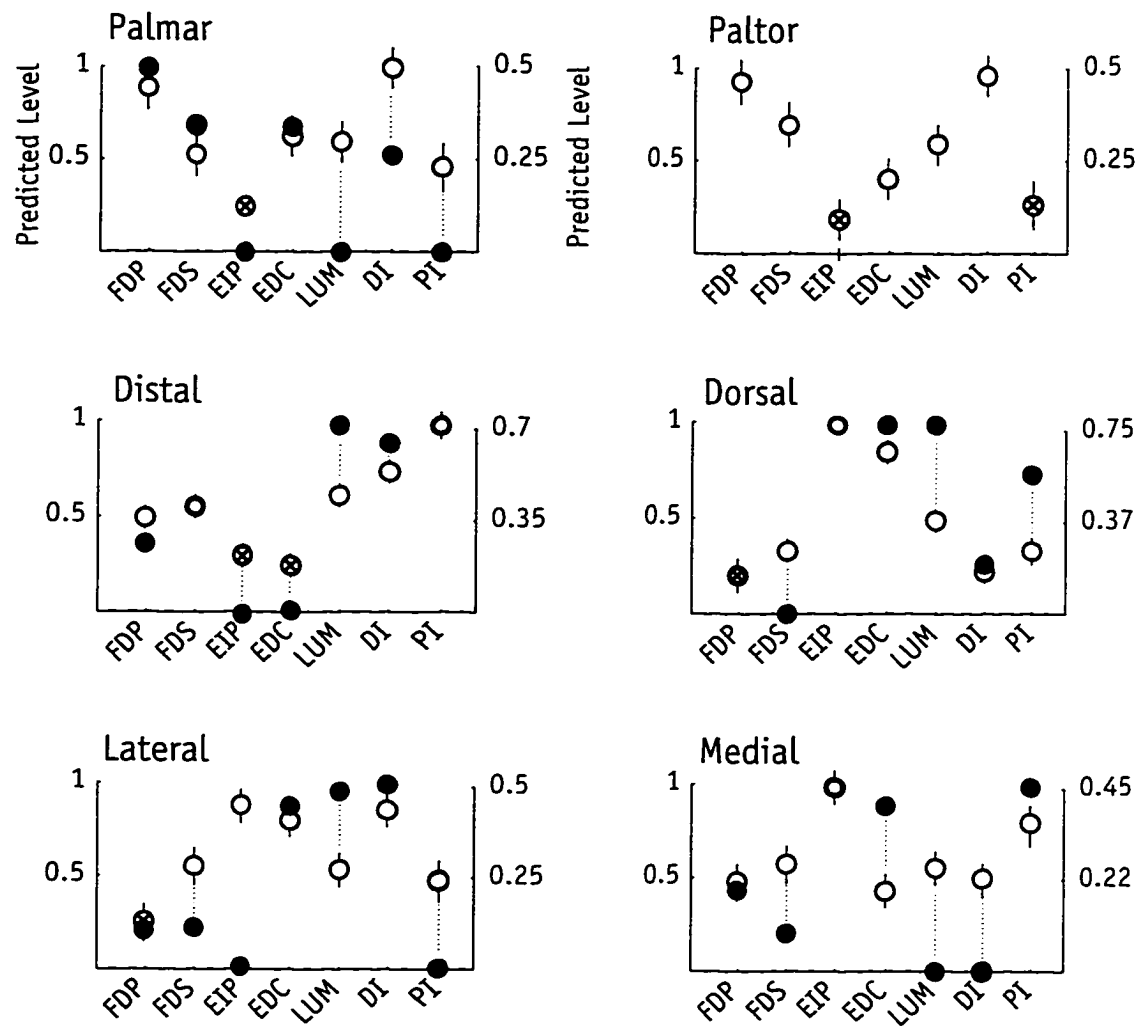
FIGURE B.2. Comparison of EMG to model-generated excitation for **intermediate posture.**
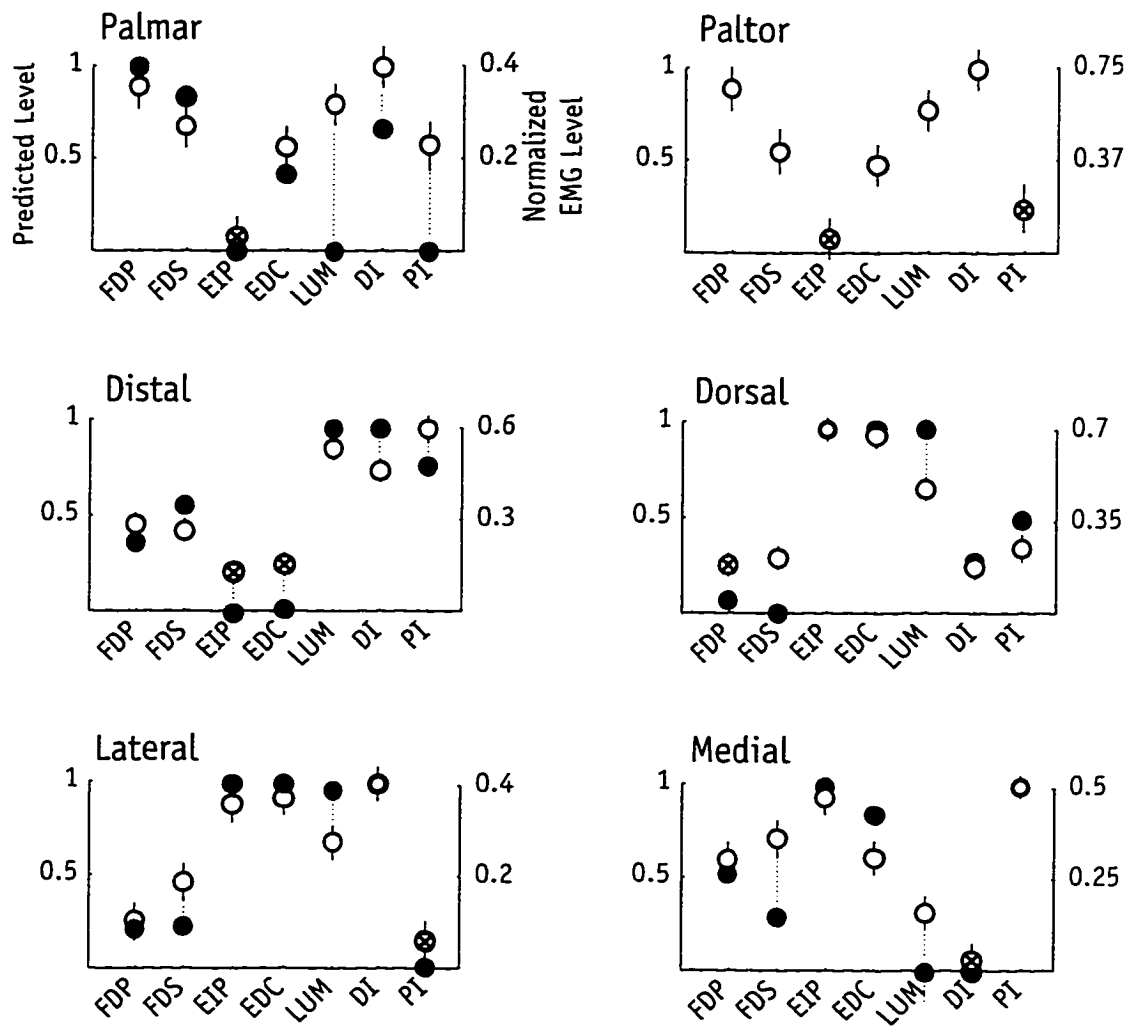
FIGURE B.3. Comparison of EMG to model-generated excitation for **extended posture.**

COMPARISON OF EXPERIMENTAL AND MODEL-

GENERATED FORCES

TABLE B.4. Finger forces, means (N)

	Direction	Predicted	Experimental		
			Mean	Std. Dev.	Std. Error
Extended	paltor	35.07	33.209	8.629	2.602
	palmar	27.04	26.333	10.861	2.804
	dorsal	9.22	6.565	2.198	.567
	medial	11.68	15.867	7.615	1.966
	lateral	10.76	14.312	8.317	2.147
	distal	108.5	25.338	12.498	3.227
Intermediate	paltor	38.3	35.509	5.514	1.662
	palmar	25.4	25.240	6.130	1.583
	dorsal	6.14	7.259	2.197	.567
	medial	11.8	20.006	10.310	2.662
	lateral	17.48	14.567	4.541	1.173
	distal	123.1	26.313	11.046	2.852
Flexed	paltor	32.34	36.018	11.394	3.435
	palmar	24.16	31.060	10.472	2.704
	dorsal	6.93	7.562	2.040	.527
	medial	23.69	21.647	9.622	2.484
	lateral	32.1	15.240	6.942	1.792
	distal	38.92	27.080	12.675	3.273

TABLE B.5. Finger Forces, adjusted (Least Squares) Means (N)

		Predicted	Experimental		
	Direction		Mean	Std. Dev.	Std. Error
Extended	paltor	35.07	33.450	6.477	1.953
	palmar	27.04	26.544	6.425	1.659
	dorsal	9.22	6.776	6.425	1.659
	medial	11.68	16.078	6.425	1.659
	lateral	10.76	14.523	6.425	1.659
	distal	108.5	25.549	6.425	1.659
Intermediate	paltor	38.3	35.750	6.477	1.953
	palmar	25.4	25.451	6.425	1.659
	dorsal	6.14	7.470	6.425	1.659
	medial	11.8	20.217	6.425	1.659
	lateral	17.48	14.778	6.425	1.659
	distal	123.1	26.524	6.425	1.659
Flexed	paltor	32.34	36.259	6.477	1.953
	palmar	24.16	31.271	6.425	1.659
	dorsal	6.93	7.773	6.425	1.659
	medial	23.69	21.858	6.425	1.659
	lateral	32.1	15.451	6.425	1.659
	distal	38.92	27.291	6.425	1.659

RELATIVE SENSITIVITY OF FORCE MAGNITUDES TO

MODEL PARAMETERS

TABLE B.6. Relative sensitivity of force magnitudes parameters, flexed posture

	Joint	Tendon	Dorsal	Palmar	Distal	Lateral	Medial
Moment arms, mm	MCP adduction (adduction +) (abduction -)	FDP	—	—	-0.21	—	0.33
		EIP	—	—	—	—	—
		EDC	—	—	—	0.11	—
		LUM	—	—	—	0.11	—
		DI	—	—	0.77	0.94	—
		PI	—	—	-0.67	—	0.18
	MCP Flexion (flexion +) (extension -)	FDP	—	-0.86	0.9	—	-1
		EIP	—	0.5	—	—	0.54
		LUM	—	—	0.14	—	—
		DI	—	—	0.23	—	—
		PI	—	—	0.37	—	—
	PIP Flexion	FDP	-0.24	1	-0.9	—	0.88
		proximal slip	1	-0.23	0.5	—	-0.33
	DIP Flexion	FDP	0.26	0.24	0.18	—	—
		terminal slip	-0.62	—	-0.17	—	—
Extensor Mechanism	Item						
	Proportion to proximal slip		0.8	-0.21	—	—	-0.23
	Top bifurcation angle		0.4	—	0.5	—	-0.1
	Bottom bifurcation angle		-0.39	—	-0.17	—	—
PCSA, cm²	Muscle						
	FDP		—	0.34	—	—	0.19
	FDS		—	—	—	—	—
	EIP		—	—	—	—	—
	EDC		0.32	0.16	—	—	0.19
	LUM		—	—	0.29	0.14	—
	DI		—	—	1	1	—
	PI		—	—	—	—	—

For adjusted model, normalized by column.

"—" indicates relative sensitivity is below 0.10.

Because we lump all excitation-independent muscle force parameters as PCSA (i.e., optimal fiber length is assumed), sensitivity to PCSA may mean that maximal force following reconstructive surgeries is sensitive to tendon resting length. Because the model cannot reproduce interosseous muscle co-excitation for lateral force, the predicted sensitivities for lateral force may not apply.

83

TABLE B.7. Relative sensitivity of force magnitudes parameters, intermediate posture

	Joint	Tendon	Dorsal	Palmar	Distal	Lateral	Medial
Moment arms, mm	MCP adduction	FDP	—	—	—	-0.11	0.34
	(adduction +)	EIP	—	—	—	—	—
	(abduction -)	EDC	—	—	—	0.12	-0.18
		LUM	—	—	—	0.1	—
		DI	—	—	—	0.98	—
		PI	—	—	—	—	1
	MCP Flexion	FDP	—	-0.67	1	—	-0.46
	(flexion +)	EIP	—	0.13	—	—	0.86
	(extension -)	LUM	—	—	—	—	—
		DI	—	—	0.12	—	—
		PI	—	—	0.17	—	—
	PIP Flexion	FDP	-0.3	1	-0.77	0.11	0.48
		proximal slip	0.98	—	0.26	—	-0.33
	DIP Flexion	FDP	0.34	0.7	—	—	-0.13
		terminal slip	-0.62	—	—	—	0.12

	Item	Dorsal	Palmar	Distal	Lateral	Medial
Extensor Mechanism	Proportion to proximal slip	1	—	—	—	-0.24
	Top bifurcation angle	0.4	—	0.26	—	—
	Bottom bifurcation angle	-0.37	—	—	—	—

	Muscle	Dorsal	Palmar	Distal	Lateral	Medial
PCSA, cm²	FDP	—	0.74	—	—	—
	FDS	—	—	—	—	—
	EIP	—	—	—	—	—
	EDC	0.31	—	—	—	0.17
	LUM	—	—	0.11	—	—
	DI	—	—	0.14	1	—
	PI	—	—	0.31	—	0.83

TABLE B.8. Relative sensitivity of force magnitudes parameters, extended posture

Joint	Tendon	Dorsal	Palmar	Distal	Lateral	Medial
MCP adduction	FDP	—	—	-0.13	-0.16	0.29
(adduction +)	EIP	—	—	—	—	—
(abduction -)	EDC	—	—	—	0.13	-0.12
	LUM	—	—	—	0.1	—
	DI	—	—	0.33	1	—
	PI	—	—	-0.24	—	1
MCP Flexion	FDP	—	-0.24	1	-0.19	-0.51
(flexion +)	EIP	0.48	0.067	—	0.54	0.85
(extension -)	LUM	—	—	—	—	—
	DI	—	—	0.29	-0.16	0.
	PI	—	—	—	—	—
PIP Flexion	FDP	-0.13	0.95	-0.93	0.33	0.62
	proximal slip	1	—	0.26	-0.32	-0.43
DIP Flexion	FDP	0.14	0.83	—	—	—
	terminal slip	-0.2	—	—	—	—

Moment arms, mm

Item		Dorsal	Palmar	Distal	Lateral	Medial
Proportion to proximal slip		0.43	—	—	-0.28	-0.25
Top bifurcation angle		0.65	—	0.26	—	—
Bottom bifurcation angle		-0.27	—	—	—	—

Extensor Mechanism

Muscle		Dorsal	Palmar	Distal	Lateral	Medial
FDP		—	1	—	—	—
FDS		—	—	—	—	—
EIP		0.3	—	—	—	—
EDC		0.93	—	—	0.2	0.1
LUM		—	—	0.16	—	—
DI		—	—	0.62	0.84	—
PI		—	—	—	—	0.95

PCSA, cm²

APPENDIX C: SAMPLE CALCULATION OF

FEASIBLE FORCE SET OF POINT-FORCES IN

THE PLANE OF FINGER FLEXION

Jacobian for index-finger

	$\delta q1$	$\delta q2$	$\delta q3$	$\delta q4$
δx	$-c1\,(c2\,l1 + c23\,l2 + c234\,l3)$	$s1\,(l1\,s2 + l2\,s23 + l3\,s234)$	$s1\,(l2\,s23 + l3\,s234)$	$l3\,s1\,s234$
δy	$-(c2\,l1 + c23\,l2 + c234\,l3)\,s1$	$-c1\,(l1\,s2 + l2\,s23 + l3\,s234)$	$-c1\,(l2\,s23 + l3\,s234)$	$-c1\,l3\,s234$
δz	0	$c2\,l1 + c23\,l2 + c234\,l3$	$c23\,l2 + c234\,l3$	$c234\,l3$
$\delta \phi$	0	1	1	1

l1, l2 and l3 are the lengths of the 1st 2nd and third metacarpals, respectively. Angle q1 is MCP ad-abduction, q2 MCP flexion, q2 proximal and q3 distal interpahalngeal joints. c1 is Cos[q1], c12 is Cos[q1+q2], etc. The Jacobian specifies the relationship between joint angular velocities $\{\partial q1, \partial q2, \partial q3$ and $\partial q4\}$ and finger tip linear $\{\delta x, \delta y$ and $\delta z)$ and angular $\{\delta\phi\}$ velocities. For a given finger posture the Jacobian is constant matrix.

Model Matrix for the flexed posture
Model = J^{-T} R

	fp	fs	di	pi	ei	lum	ec
Fx	-0.08941	-0.0447	0.2087	-0.2138	-0.009249	0.1421	0.03669
Fy	-0.04689	-0.1496	1.456×10^{-17}	0.0248	0.052	0.0248	0.052
Fz	0.06472	0.001953	0.0568	0.2067	-0.1518	0.2919	-0.1518
Tx	0.003081	-0.002352	0.0001578	-0.000685	-0.0001649	-0.0004483	-0.0001649

The Model is a constant numerical matrix at each posture. It specifies how the excitation of each muscle {fp, fs, di, pi, ei, lum, ec} is transformed into finger tip forces {fx,fy,fz} and finger output torque {tx} by the moment arms, extensor mechanism and Jacobian.

Vertices of a 7D excitation hypercube

The excitation of a muscle is described by a value between 0 and 1. Therefore, all feasible muscle excitation patterns are included in a 7D positive hypercube. Its 128 vertices (2^7) are all the possible combinations of 1's and 0's in groups of seven.

First and fourth rows of Model are constraints

Point-forces in the plane of finger flexion have, by definition, zero Fx and Tx output components. The corresponding rows of the Model, used as linear equations equal to zero, describe 7D hyperplanes whose intersection contains all possible excitations that produce point-forces in the plane of finger flexion.

	fp	fs	di	pi	ei	lum	ec
fx = 0 =	-0.08941	-0.0447	0.2087	-0.2138	-0.009249	0.1421	0.03669
tx = 0 =	0.06472	0.001953	0.0568	0.2067	-0.1518	0.2919	-0.1518

46 vertices describe the intersection of
hyperplanes in the 7D excitation hypercube

	fp	fs	di	pi	ei	lum	ec
1	1.	0.624	1.	0.547	1.	1.	1.
2	1.	0.6644	1.	0.422	1.	0.	1.
3	1.	0.6306	1.	0.5525	0.	1.	1.
4	1.	0.671	1.	0.4275	0.	0.	1.
5	1.	0.6776	1.	0.4066	1.	1.	0.
6	1.	0.7179	1.	0.2816	1.	0.	0.
7	1.	0.6842	1.	0.4121	0.	1.	0.
8	1.	0.7245	1.	0.2872	0.	0.	0.
9	0.1539	0.	1.	0.8788	0.	0.	0.
10	0.201	0.	1.	0.9709	0.	1.	0.
11	0.1616	0.	1.	0.8679	1.	0.	0.
12	0.2087	0.	1.	0.96	1.	1.	0.
13	0.2164	0.	1.	0.9755	0.	0.	1.
14	0.2241	0.	1.	0.9646	1.	0.	1.
15	0.3715	0.2177	0.	0.	1.	1.	1.
16	0.1928	0.105	0.	0.	1.	0.	1.
17	0.1173	0.	0.	0.1778	1.	1.	1.
18	0.07022	0.	0.	0.08573	1.	0.	1.
19	0.3794	0.231	0.	0.	0.	1.	1.
20	0.1097	0.	0.	0.1887	0.	1.	1.
21	0.06254	0.	0.	0.09663	0.	0.	1.
22	0.2007	0.1183	0.	0.	0.	0.	1.
23	0.04711	0.	0.	0.09203	0.	1.	0.
24	0.1787	0.1127	0.	0.	0.	1.	0.
25	0.	0.	0.	0.	0.	0.	0.
26	0.009587	0.	0.0124	0.	1.	0.	0.
27	0.01473	0.	0.	0.	1.	0.	0.1128
28	0.01326	0.	0.	0.	1.	0.1184	0.
29	0.1708	0.09935	0.	0.	1.	1.	0.
30	0.05479	0.	0.	0.08114	1.	1.	0.
31	1.	0.7629	0.7089	0.	0.	0.	0.
32	1.	0.7392	0.5822	0.	0.	1.	0.
33	1.	0.7556	0.7145	0.	1.	0.	0.
34	1.	0.7319	0.5878	0.	1.	1.	0.
35	1.	0.7281	0.5666	0.	0.	0.	1.
36	1.	0.7044	0.4399	0.	0.	1.	1.
37	1.	0.7208	0.5722	0.	1.	0.	1.
38	1.	0.6971	0.4455	0.	1.	1.	1.
39	0.2517	0.	0.9232	1.	0.	1.	1.
40	0.2613	0.	0.9356	1.	1.	1.	1.
41	0.2423	0.	1.	1.	1.	0.3849	1.
42	0.2346	0.	1.	1.	1.	1.	0.4141
43	0.3522	0.06932	1.	1.	1.	1.	1.
44	0.229	0.	1.	1.	0.	0.2665	1.
45	0.2199	0.	1.	1.	0.	1.	0.3014
46	0.3601	0.08266	1.	1.	0.	1.	1.

Point-forces in the plane of finger flexion

	Fx	Fy	Fz	Tx
1	-1.249×10^{-8}	-17.93	18.78	-1.008×10^{-9}
2	-1.056×10^{-8}	-20.19	9.145	-5.203×10^{-10}
3	-1.582×10^{-8}	-19.35	22.5	-5.681×10^{-10}
4	7.498×10^{-9}	-21.61	12.87	-1.194×10^{-11}
5	-1.94×10^{-8}	-24.9	28.97	-1.124×10^{-9}
6	-1.746×10^{-8}	-27.16	19.33	-6.36×10^{-10}
7	-2.273×10^{-8}	-26.32	32.69	-6.838×10^{-10}
8	5.919×10^{-10}	-28.58	23.05	-1.276×10^{-10}
9	5.149×10^{-8}	1.937	31.86	1.677×10^{-10}
10	-2.281×10^{-9}	2.496	41.	-2.087×10^{-11}
11	5.636×10^{-8}	3.08	28.06	3.174×10^{-10}
12	2.59×10^{-9}	3.64	37.2	1.288×10^{-10}
13	-6.604×10^{-8}	6.657	21.02	-3.164×10^{-10}
14	-6.117×10^{-8}	7.8	17.22	-1.667×10^{-10}
15	-3.854×10^{-9}	-2.745	-8.137	7.981×10^{-11}
16	-1.387×10^{-9}	1.442	-15.91	-6.661×10^{-11}
17	4.649×10^{-9}	6.423	-5.492	2.496×10^{-11}
18	-4.84×10^{-9}	5.864	-14.64	-2.276×10^{-11}
19	4.625×10^{-10}	-4.451	-4.499	-2.576×10^{-11}
20	-2.22×10^{-10}	5.28	-1.691	-1.247×10^{-10}
21	8.096×10^{-9}	4.72	-10.84	1.929×10^{-11}
22	2.929×10^{-9}	-0.2639	-12.28	-1.722×10^{-10}
23	1.038×10^{-8}	0.5597	9.146	1.691×10^{-11}
24	-2.466×10^{-9}	-4.187	7.776	1.464×10^{-10}
25	0.	0.	0.	0.
26	-6.783×10^{-10}	1.168	-3.405	2.714×10^{-13}
27	-1.357×10^{-9}	1.676	-5.023	-6.601×10^{-12}
28	-4.871×10^{-10}	1.21	-2.718	1.378×10^{-11}
29	2.158×10^{-9}	-2.482	4.138	-5.612×10^{-11}
30	-3.447×10^{-9}	1.703	5.345	5.669×10^{-12}
31	-1.878×10^{-8}	-30.76	13.31	-1.109×10^{-9}
32	-5.796×10^{-9}	-29.45	18.71	-8.074×10^{-10}
33	1.341×10^{-8}	-29.3	9.778	9.606×10^{-10}
34	-1.831×10^{-8}	-27.99	15.18	-1.089×10^{-9}
35	-1.542×10^{-9}	-24.85	-1.636	-5.066×10^{-10}
36	-9.434×10^{-9}	-23.54	3.761	-2.203×10^{-10}
37	-1.406×10^{-8}	-23.39	-5.169	-7.885×10^{-10}
38	-1.079×10^{-9}	-22.08	0.2284	-4.865×10^{-10}
39	-1.014×10^{-7}	7.068	27.72	-3.724×10^{-11}
40	8.663×10^{-8}	8.235	24.31	7.424×10^{-11}
41	3.779×10^{-9}	8.016	20.74	-1.128×10^{-10}
42	3.823×10^{-9}	5.595	32.72	-9.07×10^{-11}
43	-3.854×10^{-9}	5.44	25.52	1.826×10^{-10}
44	3.372×10^{-9}	6.806	23.46	-9.576×10^{-11}
45	-4.748×10^{-9}	3.919	37.74	1.481×10^{-10}
46	4.625×10^{-10}	3.734	29.16	7.699×10^{-11}

Feasible set of point-forces

The feasible force set is the 12-vertex convex hull of point-forces (Figure C.1). It specifies the achievable point-forces in the plane of finger flexion. The distance from the origin to the boundary indicates the maximal force that can be produced in that direction. Fy is the Distal direction, Fz the Palmar. Note that 34 excitation vertices map into the interior of the feasible force set.
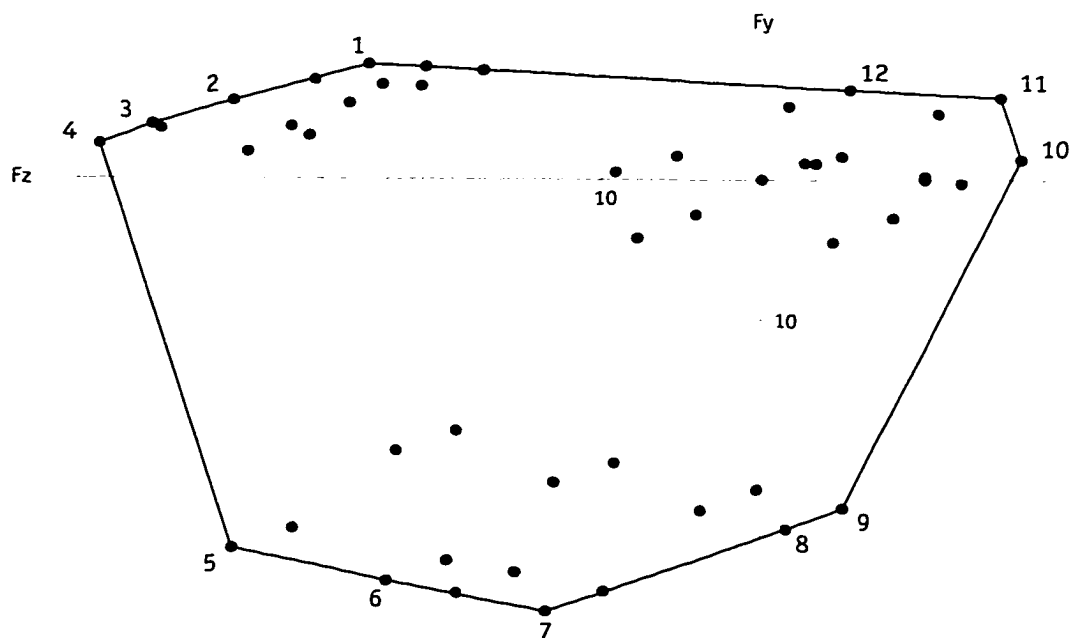
FIGURE C.1. Feasible force set

Point-force vertices (N) that define the feasible force set

	Fy	Fz
1	8.235	24.31
2	5.595	32.72
3	3.919	37.74
4	2.496	41.
5	-26.32	32.69
6	-28.58	23.05
7	-30.76	13.31
8	-24.85	-1.636
9	-23.39	-5.169
10	1.442	-15.91
11	5.864	-14.64
12	6.423	-5.492

Unique excitations that produce each point-force vertex

	fp	fs	di	pi	ei	lum	ec
1	0.2613	0.	0.9356	1.	1.	1.	1.
2	0.2346	0.	1.	1.	1.	1.	0.4141
3	0.2199	0.	1.	1.	0.	1.	0.3014
4	0.201	0.	1.	0.9709	0.	1.	0.
5	1.	0.6842	1.	0.4121	0.	1.	0.
6	1.	0.7245	1.	0.2872	0.	0.	0.
7	1.	0.7629	0.7089	0.	0.	0.	0.
8	1.	0.7281	0.5666	0.	0.	0.	1.
9	1.	0.7208	0.5722	0.	1.	0.	1.
10	0.1928	0.105	0.	0.	1.	0.	1.
11	0.07022	0.	0.	0.08573	1.	0.	1.
12	0.1173	0.	0.	0.1778	1.	1.	1.

The point forces at the boundaries are produced by unique excitation vectors. The excitation vectors that produce the vertices are known, and linear interpolation yields the unique excitation vectors that produce forces directed between any two vertices.

Maximal muscle forces, N

The maximal muscle force of each muscle is proportional to its physiological cross sectional area and the maximal stress muscle tissue can produce (30 N/cm^2).

fp	123.
fs	219.
di	124.8
pi	129.6
ei	23.52
lum	21.6
ec	91.74

LIST OF REFERENCES

Agee, J., McCarroll, H. R. and Hollister, A. M. (1991) The anatomy of the flexor digitorum superficialis relevant to tendon transfers. *J Hand Surg (B)* **16B**, 68-69.

An, K. N. (1996). *Personal communication.*

An, K. N., Chao, E. Y., Cooney, W. P. and Linscheid, R. L. (1979) Normative model of human hand for biomechanical analysis. *J Biomechanics* **12**, 775-788.

An, K. N., Chao, E. Y., Cooney, W. P. and Linscheid, R. L. (1985) Forces in the normal and abnormal hand. *J Orthop Res* **3**, 202-211.

An, K. N., Ueba, Y., Chao, W. P., Cooney, E. Y. and Linscheid, R. L. (1983) Tendon excursion and moment arm of index finger muscles. *J Biomechanics* **16**, 419-425.

Avis, D. and Fukuda, K. (1992) A pivoting algorithm for convex hulls and vertex enumeration of arrangements and polyhedra. *Discrete and Computational Geometry* 295-313.

Basmajian, J. V. and De Luca, C. J. (1985) Muscles Alive: their functions revealed by electromyography (5th Edn). Williams & Wilkins, Baltimore.

Berme, N., Paul, J. P. and Purves, W. K. (1977) A biomechanical analysis of the metacarpophalangeal joint. *J Biomechanics* **10**, 409-412.

Boivin, G., Wadsworth, G. E., Landsmeer, J. M. F. and Long, C. (1969) Electromyographic kinesiology of the hand: muscles driving the index finger. *Arch Phys Med Rehab* 17-26.

Brand, P. and Hollister, A. (1993) Clinical mechanics of the hand (2nd Edn). Mosby-Year Book, Inc, St. Louis.

Burgar, C. G. and Valero-Cuevas, F. J. (1996) Improved targeting of long finger flexors during chemodenervation. 1996 Academy Abstracts. *Arch Phys Med Rehab* 985.

Burgar, C. G., Valero-Cuevas, F. J. and Hentz, V. R. (1996) Improving selectivity of fine-wire electrode placement for kinesiological and clinical studies: Application to index finger musculature. *Am J of PM&R* , *submitted*.

Chao, E. Y. and An, K. N. (1978) Graphical interpretation of the solution to the redundant problem in biomechanics. *J Biomech Eng* **100**, 159-167.

Chu-Andrews, J. (1986) Electrodiagnosis: an anatomical and clinical approach. Lippincott, Philadelphia.

Chvátal, V. (1983) Linear Programming. W.H. Freeman and Company, New York.

Close, J. R. and Kidd, C. C. (1969) The functions of the muscles of the thumb, the index, and long fingers. Synchronous recording of motions and action potentials of muscles. *J Bone Jt Surg (A)* **51**, 1601-1620.

Cole, K. (1995). *Personal communication*.

Darling, W. G. and Cole, K. J. (1990) Muscle activation patterns and kinetics of human index finger movements. *J Neurophysiol* **63**, 1098-1108.

Darling, W. G., Cole, K. J. and Miller, G. F. (1994) Coordination of index finger movements. *J Biomechanics* **27**, 479-491.

Delagi, E. F., Perotto, A. and Thomas, H. (1981) Anatomic guide for the electromyographer—the limbs (2nd Edn). Charles C. Thomas, Springfield.

Delp, S. and Maloney, W. (1993) Effects of hip center location on the moment-generating capacity of the muscles. *J Biomech* **26**, 485-499.

Enoka, R. M. and Stuart, D. G. (1992) Neurobiology of muscle fatigue. *J Appl Physiol* 1631-1648.

Fahrer, M (1971) Considérations sur l'anatomie fonctionnelle du muscle fléchisseur commun profond des doigits. *Ann Chir*, 25, C.945-950.

93

Garcia-Elias, M., An, K. N., Berglund, L., Linscheid, R. L., Cooney, W. P. and Chao, E. Y. (1991) Extensor mechanism of the fingers: I. A quantitative geometric study. *J Hand Surg (A)* **16**, 1130-1140.

Geenen, C., Consky, E. and Ashby, P. (1996) Localizing muscles for botulinum toxin treatment of focal hand dystonia. *Can J Neurol SCi* 194-197.

Goodgold, J. (1984) Anatomical correlates of clinical electromyography (2nd Edn). Williams & Wilkins, Baltimore.

Gordon, M. E. (1990) An analysis of the biomechanics and muscular synergies of human standing, PhD Thesis, Stanford University, Stanford.

Graves, J. E. and James, R. J. (1990) Concurrent augmented feedback and isometric force generation during familiar and unfamiliar muscle movements. *Res Q Exerc Sport* **61**, 75-79.

Harding, D. C., Brandt, K. D. and Hillberry, B. M. (1993) Finger joint force minimization in pianists using optimization techniques. *J Biomechanics* **26**, 1403-1412.

Hentz, V. R., Hamlin, C. and Keoshian, L. A. (1988) Surgical reconstruction in tetraplegia. *Hand Clin* **4**, 601-607.

Hentz, V. R., House, J., McDowell, C. and Moberg, E. (1992) Rehabilitation and surgical reconstruction of the upper limb in tetraplegia: an update. *J Hand Surg [Am]* **17**, 964-967.

Ikebuchi, Y., Murakami, T. and Ohtsuka, A. (1988) The interosseous and lumbrical muscles in the human hand, with special reference to the insertions of the interosseous muscles. *Acta Med Okayama* **42**, 327-334.

Jacobson, M. D., Raab, R., Fazeli, B. M., Abrams, R. A., Botte, M. J. and Lieber, R. L. (1992) Architectural design of the human intrinsic hand muscles. *J Hand Surg [Am]* **17**, 804-809.

Keir, P. J., Wells, R. P., Ranney, D.A. (1996) Passive forearm musculature with reference to hand and finger postures. *Clin Biomech* **11**, 401-409.

Kelsey, J. L. (1984) Chapter 39: Prevalence studies of the epidemiology of osteoarthrosis. In *Epidemiology of the Rheumatic Disease* . Edited by Lawrence, R. C. and Shulman, L. E., pp. 282-288. Gower Medical Publishing, Ltd, New York.

Kuo, B. C. (1987) Automatic control systems (5th Edn). Prentice Hall, Englewood Cliffs.

Kuo, A. D. and Zajac, F. E. (1993) A biomechanical analysis of muscle strength as a limiting factor in standing posture. *J Biomechanics* **26** Suppl 1, 137-150.

Law, C. L., Berglung, L. J., Cooney, W. P. and An, K. N. (1989) Biomechanical study of tendon excursion of thumb muscles related to interphalangeal and metacarpophalangeal joint motion. *Kao-Hsiung i Hsueh Ko Hsueh Tsa Chih Kaohsiung Journal of Medical Sciences* **5**, 649-662.

Lee, J. W. and Rim, K. (1990) Maximum finger force prediction using a planar simulation of the middle finger. *Proceedings of the Institution of Mechanical Engineers Part H, Journal of Engineering in Medicine* **204**, 169-178.

Leffert, R. D. and Meister, M. (1976) Patterns of neuromuscular activity following tendon transfer in the upper limb: a preliminary study. *J Hand Surg [Am]* **1**, 181-189.

Leijnse, J. N. and Kalker, J. J. (1995) A two-dimensional kinematic model of the lumbrical in the human finger. *J Biomech* **28**, 237-249.

Lieber, R., Loren, G. and Friden, J. (1994) In vivo measurement of human wrist extensor muscle sarcomere length changes. *J Neurophysiol* **71**, 874-881.

Lieber, R. L., Jacobson, M. D., Fazeli, B. M., Abrams, R. A. and Botte, M. J. (1992) Architecture of selected muscles of the forearm: anatomy and implications for tendon transfer. *J Hand Surg (A)* **17**, 787-798.

Loeb, G. E. and Gans, C. (1986) Electromyography for experimentalists. University of Chicago Press, Chicago, ILL.

Long, C., Conrad, P. W., Hall, E. A. and Furler, S. L. (1970) Intrinsic-extrinsic muscle control of the hand in power grip and precision handling. An electromyographic study. *J Bone Joint Surg [Am]* **52**, 853-867.

Maier, M. A. and Hepp-Reymond, M. C. (1995a) EMG activation patterns during force production in precision grip. I. Contribution of 15 finger muscles to isometric force. *Exp Brain Res* **103**, 108-122.

Maier, M. A. and Hepp-Reymond, M. C. (1995b) EMG activation patterns during force production in precision grip. II. Muscular synergies in the spatial and temporal domain. *Exp Brain Res* **103**, 123-136.

Mathiowetz, V., Kashman, N., Volland, G., Weber, K., Dowe, M. and Rogers, S. (1985) Grip and pinch strength: normative data for adults. *Arch Phys Med Rehab* **66**, 69-74.

McFarlane, R. M. (1987) Unsatisfactory results in hand surgery. Edited by McFarlane, R. M., Churchill Livingstone, New York.

Minami, A., An, K. N., Cooney, W. P., Linscheid, R. L., Chao, E. Y. (1985) Ligament stability of the metacarpophalangeal joint: a biomechanical study. *J Hand Surg (A)* **10**, 255-60.

Moberg, E. (1990) Chapter 116: Surgery for the spastic, stroke and tetraplegic hand. In *Plastic Surgery* v8 part 2 (First Edn). Edited by McCarthy, J., pp. 4977-4990. W.B. Saunders Company, Philadelphia.

O'Driscoll, S. W., Horii, E., Ness, R., Cahalan, T. D., Richards, R. R. and An, K. N. (1992) The relationship between wrist position, grasp size, and grip strength. *J Hand Surg (A)* **17**, 169-177.

Park, T. A. and Harris, G. F. (1996) "Guided" intramuscular fine wire electrode placement. A new technique. *Am J Phys Med Rehabil* **75**, 232-234.

Perotto, A. O. (1994) Anatomic Guide for the Electromyographer: The Limbs and Trunk (3rd Edn). Charles C. Thomas, Springfield.

Spoor, C. W. (1983) Balancing a force on the fingertip of a two dimensional finger model without intrinsic muscles. *J Biomechanics* **16**, 497-504.

Storace, A. and Wolf, B. (1982) Kinematic analysis of the role of the finger tendons. *J Biomechanics* **15**, 391-393.

Thompson, D. E., Buford, W. L., Myers, L. M., Giurintano, D. J. and Brewer, J. A. (1988) A hand biomechanics workstation. *Computer Graphics* **22**, 335-343.

Tubiana, R. (1981) The Hand. Edited by Tubiana, R., Saunders, Philadelphia.

Valero-Cuevas, F. J. (1997) Implications of metacarpophalangeal joint kinematics to the force

production capabilities of a 3D index-finger model. In *ASME Summer Bioengineering*

Conference, Sun River, Oregon.

Valero-Cuevas, F. J., Burgar, C., Zajac, F. E., Hentz, V. R., McGill, K. C. and An, K. N. (1996) Muscle

coordination during maximal index-finger ad-abduction forces. In *26th Annual Meeting of the*

Society for Neuroscience, Washington, D.C.

Weightman, B. and Amis, A. (1982) Finger joint force predictions related to design of joint

replacements. *J Biomed Eng* **4**, 197-205.

Williams, P. L. (1995) Gray's anatomy : the anatomical basis of medicine and surgery. Edited by

Williams, P. L., Churchill Livingstone, New York.

Yoshikawa, T. (1990) Foundations of robotics: analysis and control. The MIT Press, Cambridge.

Youm, Y., Gillespie, T. E., Flatt, A. E. and Sprague, B. L. (1978a) Kinematic investigation of normal

MCP joint. *J Biomechanics* **11**, 109-118.

Youm, Y., McMurtry, R. Y., Flatt, A. E. and Sprague, B. L. (1978b) Kinematics of the wrist—I. An

experimental study of radial-ulnar deviation and flexion-extension. *Journal of Bone and Joint*

Surgery **A60**, 423-431.

Zajac, F. E. (1989) Muscle and tendon: properties, models, scaling, and application to

biomechanics and motor control. *Crit Rev Biomed Eng* **17**, 359-411.

Zajac, F. E. (1992) How musculotendon architecture and joint geometry affect the capacity of

muscles to move and exert force on objects: a review with application to arm and forearm

tendon transfer design. *J Hand Surg (A)* **17**, 799-804.

Zancolli, E. (1979) Structural and dynamic bases of hand surgery (2nd Edn). Lippincott,

Philadelphia.